

# 1 Long-range transport of stratospheric aerosols in the 2 Southern Hemisphere following the 2015 Calbuco eruption

3 Nelson Bègue<sup>1</sup>, Damien Vignelles<sup>2</sup>, Gwenaël Berthet<sup>2</sup>, Thierry Portafaix<sup>1</sup>, Guillaume  
4 Payen<sup>1</sup>, Fabrice Jégou<sup>2</sup>, Hassan Benchérif<sup>1,6</sup>, Julien Jumelet<sup>3</sup>, Jean-Paul Vernier<sup>4</sup>,  
5 Thibaut Lurton<sup>2</sup>, Jean-Baptiste Renard<sup>2</sup>, Lieven Clarisse<sup>5</sup>, Vincent Duverger<sup>2</sup>, Françoise.  
6 Posny<sup>1</sup> Jean-Marc Metzger<sup>1</sup> and Sophie Godin-Beekmann<sup>3</sup>

7 [1] Laboratoire de l'Atmosphère et des Cyclones, UMR 8105 CNRS, Université de la Réunion,  
8 Reunion Island, France.

9 [2] Laboratoire de Physique et Chimie de l'Environnement et de l'Espace, Université d'Orléans,  
10 CNRS/INSU UMR7328, Orléans, France

11 [3] Laboratoire Atmosphère Milieux Observations Spatiales, University of Paris VI, Paris,  
12 France

13 [4] NASA Langley Research Center, Hampton, Virginia, USA

14 [5] Spectroscopie de l'Atmosphère, Service de Chimie Quantique et Photophysique, Université  
15 Libre de Bruxelles, Brussels, Belgium

16 [6] School of Chemistry and Physics, University of KwaZulu-Natal, Westville, Durban, South  
17 Africa

18 Correspondence to: N.Bègue ([nelson.begue@univ-reunion.fr](mailto:nelson.begue@univ-reunion.fr))

## 19 Abstract

20 After 43 years of inactivity, the Calbuco volcano which is located in the southern part of Chile  
21 erupted on 22 April 2015. The space-time evolutions (distribution and transport) of its aerosol  
22 plume are investigated by combining satellite (CALIOP, IASI, OMPS), in situ aerosol counting  
23 (LOAC OPC) and LiDAR observations, and the MIMOSA advection model. The Calbuco  
24 aerosol plume reached the Indian Ocean **one** week after the eruption. Over the Reunion Island  
25 site (21°S; 55.5°E), the aerosol signal was unambiguously enhanced in comparison with  
26 “background” conditions with a volcanic aerosol layer extending from 18 km to 21 km during  
27 the May-July period. All the data reveal an increase by a factor of ~2 in the **sAOD** (stratospheric  
28 Aerosol Optical Depth) with respect to values observed before the eruption. **The aerosol mass  
29 e-folding time is approximately 90 days which is rather close to the value (~80 days) reported**

1 for the Sarychev eruption. Microphysical measurements obtained before, during and after the  
2 eruption reflecting the impact of the Calbuco eruption on the lower stratospheric aerosol content  
3 have been analyzed over the Reunion Island site. During the passage of the plume, the volcanic  
4 aerosol was characterized by an effective radius of  $0.16 \pm 0.02 \mu\text{m}$  with a unimodal size  
5 distribution for particles above  $0.2 \mu\text{m}$  diameter. Particle concentrations for sizes larger than  $1$   
6  $\mu\text{m}$  are too low to be properly detected by the LOAC OPC. The aerosol number concentration  
7 was  $\sim 20$  times that observed before and one year after the eruption. According to OMPS and  
8 LiDAR observations, a tendency toward conditions before the eruption has been observed by  
9 April 2016. The volcanic aerosol plume is advected eastward in the southern hemisphere and  
10 its latitudinal extent is clearly bounded by the subtropical barrier and the polar vortex. The  
11 transient behavior of the aerosol layers observed above Reunion Island between May and July  
12 2015 reflects an inhomogeneous spatio-temporal distribution of the plume which is controlled  
13 by the localization of these dynamical barriers.

## 14 1. Introduction

15 Stratospheric aerosol affect the chemical and radiation balance of the atmosphere (McCormick  
16 et al., 1995; Solomon, 1999; SPARC 2006). The importance of stratospheric aerosol on the  
17 chemistry is mostly due to its role in the ozone budget (Solomon et al., 1986; Bekki, 1997;  
18 Borrmann et al., 1997). Stratospheric aerosol provide sites for heterogeneous chemical reactions  
19 leading to stratospheric ozone depletion, significantly enhanced in periods of high aerosol  
20 loadings following major volcanic eruptions (Solomon, 1999 and references therein). In  
21 addition, periods of enhanced stratospheric aerosol loadings can lead to significant warming in  
22 the stratosphere and cooling in the troposphere (e.g. McCormick et al., 1995; Solomon et al.,  
23 2011; Arfeuille et al., 2013). As reported by Kremser et al. (2016), a better understanding of  
24 the processes governing the lifetime of stratospheric aerosol is needed to assess the impacts on  
25 climate and chemistry. Since the discovery of the permanent stratospheric aerosol layer, called  
26 Junge Layer, in 1961 (Junge, 1961), it has been established that stratospheric aerosol are mostly  
27 composed of sulfuric acid droplets with some more complex characteristics in the stratosphere  
28 where organic compounds and meteoritic dust can also contribute to its composition (Neely et  
29 al., 2011, Froyd et al., 2009). The main sources of stratospheric sulfur are Carbonyl Sulfide  
30 (OCS), Dimethyl Sulfide (DMS) and sulfur dioxide ( $\text{SO}_2$ ) (SPARC, 2006), the latter being  
31 significantly enhanced after volcanic eruptions (Carn et al., 2015). The injected  $\text{SO}_2$  into  
32 stratosphere is oxidized into  $\text{H}_2\text{SO}_4$ , which (after homogeneous nucleation and/or condensation  
33 onto existing aerosol particles) causes an increase in the content of liquid sulfate aerosol

1 (SPARC, 2006). Based on the control of the stratospheric aerosol burden over the last 25 years,  
2 Thomason et al. (2007) showed that volcanic effects dominate over natural and anthropogenic  
3 sources. Previous studies on stratospheric aerosol have significantly characterized its properties  
4 and variability during “background” (i.e. free of volcanic aerosol) and volcanic conditions (e.g.,  
5 Stenchikov et al., 1998; Jäger and Deshler, 2002; Bauman et al., 2003; Hermann et al; 2003;  
6 Hofmann et al; 2009).

7 The eruption of the Pinatubo in 1991 is known to be the last major volcanic eruption injecting  
8 between 14 and 23 Tg of SO<sub>2</sub> significantly perturbed the global stratosphere for several years  
9 (Kinninson et al., 1994; McCormick et al., 1995; Stenchikov et al., 1998, 2002; Guo et al.,  
10 2004; Dhomse et al., 2014). As reported by Russell et al. (1996), in addition to the prodigious  
11 increase in the stratospheric aerosol loading, this event significantly affected numerous aspects  
12 of the atmospheric system including: i) a 2-year cooling of the global surface temperature of  
13 several tenths of degrees (Canty et al., 2013; Wunderlich and Mitchell, 2017); ii) a warming of  
14 the tropical stratosphere ranging from 1° to 4°C (Labitzke and McCormick et al., 1992; Young  
15 et al., 1994); (iii) a lifting of the tropical ozone layer by ~1.8 km (Pueschel et al., 1992; Grant  
16 et al., 1994). By the use of satellite and balloon-borne observations, various studies have shown  
17 that moderate volcanic eruptions (i.e., volcanic explosive index less or equal to 4) can  
18 significantly modulate stratospheric aerosol concentrations (Bourassa et al., 2010; Kravitz et  
19 al., 2010; Solomon et al., 2011; Vernier et al., 2011; Clarisse et al., 2012; Jégou et al., 2013).  
20 Based upon satellite observations, Vernier et al (2011) showed that the decadal increase in  
21 stratospheric aerosol loadings since 2002 can be attributed to a series of moderate volcanic  
22 eruptions. As reported by Kremser et al (2016), this decadal trend was also obtained from  
23 LiDAR (Hofmann et al., 2009; Trickl et al., 2013; Zuev et al., 2017) and ground-based sun-  
24 photometer observations (Ridley et al., 2014). Three moderate volcanic eruptions are ranked in  
25 the top 10 of the most influential events on the stratospheric aerosol burden including during  
26 the 2002-2012 period : (1) The Kasatochi eruption (52.2° N; 175.5° W, Alaska) in 2008 which  
27 injected 1.5-2.5 Tg of SO<sub>2</sub> into the upper troposphere and lower stratosphere (UTLS) (Bourassa  
28 et al., 2010; Kravitz et al., 2010; Krotkov et al., 2010); (2) The Sarychev eruption in June 2009  
29 (48.1°N; 153.2°E, the Kuril Island) which released 0.9 Tg of SO<sub>2</sub> into the UTLS (Clarisse et al.,  
30 2012; Kravitz et al., 2011; Jégou et al., 2013); (3) The Nabro eruption (13.4°N; 41.7°E, Eritrea)  
31 in June 2011 which emitted 1.3 Tg of SO<sub>2</sub> into the UTLS (Bourassa et al., 2012; Sawamura et  
32 al; 2012). In comparison, these recurrent moderate volcanic eruptions injected 10-20 times less  
33 SO<sub>2</sub> than the Pinatubo eruption (Solomon et al., 2011). These eruptions can also be used to

1 understand stratospheric dynamics as was done for the case of the Pinatubo eruption (Trepte et  
2 al., 1992).

3 Indeed, following a volcanic eruption, stratospheric aerosol can be used as a dynamical tracer  
4 (Bencherif et al., 2003; Fairlie et al., 2014). Based on satellite observations and a Lagrangian  
5 trajectory model, Fairlie et al. (2014) used the dispersion of the Nabro plume to study the  
6 dynamics of the Asian Monsoon Anticyclone. Hitchman et al. (1994) and SPARC (2006)  
7 suggested that the stratospheric aerosol distributions could be used to understand changes in the  
8 Brewer-Dobson Circulation. More recently, Ray et al. (2014) combined in situ balloon  
9 observations of SF<sub>6</sub>, CO<sub>2</sub> with a numerical model to show that major explosive volcanic  
10 eruptions can induce large-scale changes in the stratospheric circulation via radiative  
11 perturbations, improving our understanding of stratospheric transport variability. Aerosol  
12 heating in the lower stratosphere induces a westerly wind anomaly, and enhanced tropical  
13 upwelling (Ray et al., 2014; Pitari et al., 2016a). Using the University of L'Aquila climate-  
14 chemistry model (ULAQ-CCM), Pitari et al. (2016a) analyzed the volcanic aerosol perturbation  
15 from the eruption of Mt. Pinatubo on the transport of long-lived species, N<sub>2</sub>O and CH<sub>4</sub>. They  
16 showed that the observed decline of long-lived greenhouse gases one year after the eruption is  
17 quantitatively consistent with enhanced stratosphere-troposphere exchange, due to a change in  
18 the Brewer–Dobson circulation. They also revealed that the volcanic aerosol radiative  
19 perturbation to stratospheric dynamics may be found by looking at the stratospheric age-of-air.  
20 According to Pitari et al (2016a), enhanced tropical upwelling tends to decrease the tropical age  
21 of air and the latitudinal age gradient after major volcanic eruptions. Although most studies  
22 discuss major tropical eruptions and their induced dynamical effects, we cannot exclude the  
23 possibility that extratropical eruptions in the last 15 years may also have had a significant role  
24 in lower stratospheric trends of key dynamical quantities (Kremser et al., 2016).

25 Previous works have also revealed that stratospheric aerosol can be used to study meridional  
26 air mass transport from the tropical stratospheric reservoir (Trepte and Hitchman, 1992; Randel  
27 et al., 1993; Chen et al., 1994; Grant et al., 1996, Vernier et al., 2009). Based on satellite  
28 observations, Trepte and Hitchman (1992) have shown that transport from the tropics to mid-  
29 latitudes is favored during westerly shear phases of the quasi-biennial oscillation (QBO) rather  
30 than during the easterly shear phases. More recently, by the use of satellite observations and  
31 climate models, Hommel et al. (2015) revealed that the vertical and latitudinal extent of the  
32 stratospheric aerosol layer (between 16 and 31 km) in the tropics is modulated by the QBO.  
33 Pitari et al. (2016b) analyzed the radiative perturbations in the stratosphere induced by the last

1 five major volcanic eruptions after 1960 (i.e, Agung, St Helens, El Chicon, Nevado del Ruiz  
2 and Pinatubo) using a climate model which included an aerosol microphysics module for  
3 aerosol formation and growth. They found an increase in stratospheric temperature associated  
4 with a significant impact on the tropical upwelling. The impact on stratospheric upwelling is  
5 found to be larger when the volcanically perturbed stratospheric aerosol is confined to the  
6 tropics, as tends to be the case for eruptions which are followed for several months with easterly  
7 shear of the QBO. They showed that the Nevado del Ruiz and Pinatubo eruptions occurred  
8 during years with dominant QBO easterly shear, which led to the confinement of the aerosols  
9 near the equator, with less poleward transport. This tropical confinement produced a larger  
10 latitudinal gradient of the perturbation heating rate and a stronger impact on the tropical  
11 upwelling (Pitari et al., 2016b). It is worth noting that the life cycle of an aerosol is affected by  
12 sedimentation. The fact that sulphuric particles grow larger following major eruptions (e.g.  
13 Russell et al., 1996; Bauman et al., 2003) means they can sediment appreciably during transport  
14 within the stratosphere, causing the plume transport to diverge from the expected isentropic  
15 trajectory. Even in moderate eruptions, where sulphuric particle growth may not be significant,  
16 the accommodation of sulphur on to ultra-fine ash particles has the potential to also change the  
17 fate of a proportion of the volcanic plume.

18 This paper reports on the Calbuco plume observations over Reunion Island (20.5°S; 55.5°E) and  
19 its transport in the southern tropics. The geometrical and optical properties of the Calbuco  
20 plume are inferred from the ground-based observations at Reunion Island in the framework of  
21 the MORGANE (Maïdo ObservatoRy Gas Aerosols NDACC Experiment) campaign. **The aim**  
22 **of this study is to provide a description of the dynamical context which has favored the spread**  
23 **of the Calbuco plume in the southern hemisphere.** The paper is organized as follows: Section 2  
24 describes the observations and the model used for the investigation of the volcanic aerosol  
25 transport. A description of the long-range transport of the volcanic plume over the Indian Ocean  
26 is provided in Section 3; Section 4 gives a dynamical analysis of this case study; and the  
27 summary and the conclusions are given in Section 5.

## 28 **2. Instrumentation and model description**

### 29 **2.1 Observations**

#### 30 **2.1.1 Ground-based lidar**

31 One part of the observations used in this study was performed during the MORGANE campaign  
32 which took place at the Maïdo observatory on Reunion Island in May 2015. The MORGANE

1 ground-based observational systems combine LiDAR and balloon-borne payloads to study the  
2 composition and the dynamics of the UTLS in the southern hemisphere. Among measurement  
3 data from four LiDAR systems operated during this campaign, we used data from the  
4 Differential Absorption Lidar (DIAL) system built for stratospheric ozone monitoring (Baray  
5 et al., 2013). It is also possible to retrieve aerosol profiles in the 15-38 km altitude range from  
6 these measurements. This instrument has been in operation at the Maïdo observatory since early  
7 2013. The technical details and evaluation of its performance are given by Baray et al., (2013).  
8 A brief description of this DIAL system follows. It uses a frequency-tripled Nd:YAG laser,  
9 which provides a beam at 355 nm wavelength, with a repetition rate of 30 Hz and a XeCl  
10 excimer laser which emits radiation at 308 nm at 40 Hz. The optical receiver is a telescope  
11 composed of 4 parabolic mirrors where the backscattered signal is collected by 4 optical fibers  
12 located at the focal points. The current configuration of the DIAL LiDAR system mainly detects  
13 signals in the UV regions of the spectrum (308, 332, 355 and 387 nm). The LiDAR data set  
14 used in this study consists of daily records of backscattering signal obtained from the Maïdo  
15 facility between 1 November 2014 and 30 November 2016 (106 profiles). It should be noted  
16 that no measurements were recorded at Reunion Island from January to April 2016 because of  
17 technical problems. The daily measurements are nighttime and time-integrated over about 3  
18 hours in average.

19 We used the methodology described by Sasano (1985) to obtain the extinction and backscatter  
20 coefficient from a Rayleigh-Mie LiDAR. This methodology is similar to the approach of Klett  
21 (1981) with the advantage of providing a numerical calculation of the extinction and backscatter  
22 coefficient. Temperature and pressure profiles are needed to retrieve optical properties from  
23 this approach. For this study temperature and pressure profiles obtained from a radiosondes  
24 launched from the airport of Gillot at 11h (UTC) are used. In order to obtain a complete  
25 temperature and pressure profiles range from ground to mesosphere, we used the Arletty  
26 atmospheric model (Hauchecorne et al., 1998; Nair et al., 2012), based on European Centre for  
27 Medium Range Weather Forecast (ECMWF) data. The altitude of reference is determined for  
28 each profile. On average, the reference altitude is located between 30 and 40 km. Another  
29 parameters that we need to retrieve the optical properties is the ratio of backscatter and the  
30 extinction coefficient for aerosol, also called lidar ratio. For background stratospheric aerosol,  
31 the value found in the literature is near 60 (Trickl et al., 2013 ; Ridley et al., 2014; Sakai et al.,  
32 2016; Khaykin et al., 2017). This value is commonly used for volcanically quiescent conditions  
33 and periods of moderate eruptions (Sakai et al., 2016). The LiDAR ratio depends on the particle

1 size distribution and the type of aerosol (Jäger and Deshler, 2002 ; Young and Vaughan, 2009).  
2 Error in the LiDAR ratio could influence significantly the uncertainty on aerosol extinction and  
3 optical depth (Sakai et al., 2016 ; Khaykin et al., 2017). Moreover, it should be noted that new  
4 approaches to derive extinction from LiDAR, which also measure depolarization, have been  
5 developed and already applied to space-borne lidar such as CALIOP (Young and Vaughan,  
6 2009).

### 7 **2.1.2 Balloon-borne OPC.**

8 In order to analyze the evolution of the concentration and the size of the observed aerosol over  
9 the Reunion Island site, many LOAC (Light Optical Aerosols Counter) systems were launched  
10 together with balloon-ozonesondes. A detailed description of the LOAC is given by Renard et  
11 al. (2016). In brief, LOAC is a lightweight Optical Particle Counter (OPC) of 1 kg which can  
12 fly under latex weather balloons. Through the measurements of the light scattered by particles  
13 at two specific angles (Lurton et al. 2014), the LOAC provides aerosol concentrations and  
14 particle size distributions for 19 size classes ranging from 0.2  $\mu\text{m}$  to 50  $\mu\text{m}$  in diameter every  
15 ten seconds with a vertical resolution of nearly 50 m depending on the ascent rate of the balloon.  
16 The number concentration range is from 0.6 to a few thousand particles per  $\text{cm}^3$  (Vignelles,  
17 2017). Uncertainties on number concentration during the ascent under meteorological balloon  
18 are mainly due to temperature variation effects on electronics (Renard et al., 2016, Vignelles,  
19 2017). Uncertainties on number concentrations for size bins smaller than 1  $\mu\text{m}$  is estimated to  
20 be  $\pm 30\%$ . For larger size bins, uncertainties on number concentration are governed by Poisson  
21 statistics and estimated to be  $\pm 20\%$  and  $\pm 60\%$  at particle concentrations lower than  $10^{-1}$  and  
22  $10^{-2} \text{ cm}^{-3}$ .

### 23 **2.1.3 CALIOP**

24 The Cloud-Aerosols Lidar with Orthogonal Polarization (CALIOP) on board The Cloud-  
25 Aerosols Lidar and Infrared Pathfinder Satellite Observation (CALIPSO) was used to study the  
26 transport of the Calbuco plume. CALIPSO was launched to a Sun-synchronous polar orbit in  
27 2006 (Winkler et al., 2009) with a repeat cycle of 16 days. CALIPSO is composed of an Infrared  
28 Imager Radiometer (IIR), a wide field visible camera and the CALIOP LiDAR. CALIOP is a  
29 two-wavelength polarization-sensitive LiDAR (532 and 1064 nm) which measures total  
30 attenuated backscatter vertical profiles with altitude-varying vertical (30-300 m) and horizontal  
31 (300-5000 m) resolution (Winker et al., 2009). The data used in this study are the total and  
32 perpendicular backscatter coefficient at 532 nm, available from the CALIOP level 1B V4.01

1 product. These data have been averaged every 1 degree in latitude for each orbit and grouped  
2 into data files containing 16 days of measurements. From there, the scattering ratio and  
3 depolarization ratio at 532 nm have been calculated (Vernier et al., 2009). Through the use of  
4 this algorithm, the full zonal means of scattering ratio between 20°S and 20°N are obtained by  
5 averaging 7200 cells, leading to a precision of  $\pm 1.6\%$  (Vernier et al., 2009). The ability of  
6 CALIOP to detect small volcanic plumes in the lower tropical stratosphere has been highlighted  
7 in previous studies (Thomason et al., 2007; Vernier et al., 2009, 2011).

#### 8 **2.1.4 IASI**

9 The Infrared Atmospheric Sounding Interferometer (IASI) observations were used to quantify  
10 the amount of SO<sub>2</sub> emitted during the Calbuco eruption. IASI is a nadir view thermal infrared  
11 sounder on board the Meteorological Operational satellite (MetOp-A and MetOp-B). The IASI  
12 observations used in this study were realized from the MetOp-A platform which launched in  
13 October 2006. The IASI global spatial coverage and footprint of 12 km make it relevant for  
14 monitoring of the key atmospheric species, in particular for the volcanic SO<sub>2</sub> (Clarisse et al.,  
15 2008, 2012; Clerbaux et al., 2009). The amount and altitude of emitted SO<sub>2</sub> were obtained from  
16 the algorithms detailed in Clarisse et al. (2012) and Clarisse et al. (2014) respectively. For each  
17 IASI observation, the altitude was estimated first, after which the column was calculated using  
18 the altitude information as an input parameter.

#### 19 **2.1.5 OMPS**

20 The Ozone Mapper and Profiler Suite (OMPS) Limb Profiler (LP) is also used in the present  
21 study to analyze the optical properties of the volcanic plume over the Reunion Island site.  
22 OMPS was launched on October 2011 on board the Suomi National Polar Partnership (NPP)  
23 spacecraft. The data used in this study are the daily extinction profiles at 675 nm. A detailed  
24 description of the aerosol extinction retrieval algorithm is given by Jaross et al. (2012) and  
25 Rault and Loughman (2013). Briefly, the aerosol extinction profiles are retrieved from the  
26 scattering solar radiation. The aerosol extinction are retrieved using spectral channels with weak  
27 gaseous absorption. Rodgers' maximum likelihood technique is used to retrieve the aerosol  
28 extinction profiles independently for each wavelength  $\lambda$  (Taha et al., 2011). We used 2 years  
29 (From November 2014 to November 2016) of satellite overpasses above the LiDAR site, within  
30 a 5°x5° in latitude and longitude grid. OMPS data have already used to be very effective at  
31 detecting and characterizing major events, such as the Chelyabinsk bolide in February 2013  
32 (Gorkavyi et al., 2013).



## 2.2 MIMOSA model

The Modèle Isentropique de transport Mésoéchelle de l'Ozone Stratosphérique par Advection (MIMOSA) model (Hauchecorne et al., 2002) is a Potential Vorticity (PV) advection model running on isentropic surfaces (surface of constant potential temperature). The advection scheme is semi-Lagrangian with a time step of 1 hour. The re-gridding onto the original orthonormal grid is performed every 6 hours. The model resolution is  $0.5^\circ \times 0.5^\circ$ . The advection is driven by ECMWF meteorological analyses at a resolution of  $0.5^\circ \times 0.5^\circ$ . In the case of the PV, its slow diabatic evolution is taken into account by relaxing the model PV towards the PV calculated from the ECMWF fields with a relaxation time of 10 days. Using this procedure, it is possible to run the model continuously and follow the evolution of PV filaments for several months. The accuracy of the model has been evaluated by Hauchecorne et al. (2002) and validated against airborne lidar ozone measurements using a correlation between PV and ozone, a quasi-conserved chemical tracer on timescales of a week or so within most of lower stratosphere (Heese et al., 2001; Jumelet et al., 2009). The MIMOSA model can also be used to determine the origin of air masses influencing a given site, similar to an isentropic Lagrangian trajectory model. The MIMOSA model is frequently used to detect the origin of air masses inducing laminae on ozone profiles (Hauchecorne et al., 2002; Godin et al., 2002; Portafaix et al., 2003).

## 2.3 DyBAL code

The Dynamical Barrier Location (DyBAL) code is an original software developed at the Laboratoire de l'Atmosphère et des Cyclones (LACy, France) to detect barriers to mixing in the subtropical stratosphere (Portafaix et al., 2003). The dynamical barriers are detected from the equivalent length of the tracer contour and the gradient of isentropic Ertel's potential vorticity (PV) in equivalent latitude coordinate as defined by Nakamura (1996). These two diagnostic tools are used by DyBAL to identify weak mixing and transport barriers. The position of the dynamical barrier is characterized by a local maximum of the PV gradient and a local minimum of the equivalent length (Nakamura, 1996). The DyBAL code is applied to the PV map obtained from the MIMOSA model runs. The ability of DyBAL to detect the position and the deformation of the dynamical barriers has been highlighted in previous studies (Bencherif et al., 2007; Morel et al., 2005; Portafaix et al., 2003).

## 3. Long-range transport and evolution of the Calbuco volcanic plume over the Indian Ocean

### 3.1 Plume formation and transport

#### 3.1.1 SO<sub>2</sub> plume

After 43 years of inactivity, the Calbuco erupted on 22 April 2015 and two intense explosive events were recorded during the same week. The evolution of the SO<sub>2</sub> total mass measured by IASI between 23 April 2015 and 31 May 2015 is reported in Figure 1. The SO<sub>2</sub> total mass is defined as the sum of SO<sub>2</sub> mass over the atmospheric column from midday to midnight over the southern hemisphere. As expected an increase of the SO<sub>2</sub> amounts was observed by IASI a few days following the Calbuco eruption. One day after the eruption the SO<sub>2</sub> total mass was 10 times higher than background levels. The SO<sub>2</sub> total mass increased quickly to its maximum value (0.41 Tg) on 25 April 2015 and slowly decreased to reach values close to the background values on 19 May 2015 (Fig. 2). The SO<sub>2</sub> e-folding time was estimated to be about 11 days that is in agreement with the time value reported for the 2009 Sarychev volcanic eruption (Jégou et al., 2013). The SO<sub>2</sub> total mass increased again on 28 May 2015 to reach a secondary maximum (0.13 Tg) on 30 May 2015. This new increase of the SO<sub>2</sub> total mass could be due to the Wolf eruption (Isabela Island, Galapagos) which occurred on 25 May 2015 (Xu et al., 2016). The amount of SO<sub>2</sub> emitted during the Calbuco eruption is about two times lower than the SO<sub>2</sub> mass emitted from the Sarychev eruption (0.9 Tg) in June 2009 (Jégou et al., 2013). It is also worth noting that the SO<sub>2</sub> mass injected during the Calbuco eruption is of the same order as for the Grimsvötn eruption in May 2011 (Clarisse et al., 2011). Figure 2 also depicts the maximum altitude of SO<sub>2</sub> over the period from 23 April 2015 to 31 May 2015. On average the maximum altitude of SO<sub>2</sub> is located in the lower stratosphere region around 17 km.

The SO<sub>2</sub> measurements integrated from midday to midnight obtained from IASI are also used to describe the transport of the volcanic plume over the southern hemisphere (Fig. 2). On 23 April 2015, a part of the Calbuco plume passed close to the Uruguay coast at an altitude of 17 km and then was transported by the general circulation. The plume reached Southern Africa and East side of Madagascar on 1 May 2015 at altitude of 17-18 km and was organized following a cyclonic rolling (Fig. 2b). On 6 May, the plume is mainly located over the Indian Ocean near the east coast of South Africa and partly over Namibia and South Africa. As expected, the SO<sub>2</sub> plume extent and amplitude began to diminish on 11 May 2015 by the oxidation of SO<sub>2</sub> to gaseous sulphuric acid which further converted into H<sub>2</sub>SO<sub>4</sub>-H<sub>2</sub>O liquid

1 aerosol. The plume was embedded in a thin 15-17 km altitude atmospheric layer, extending  
2 from the Atlantic Ocean to the Indian Ocean passing over the Cape of Good Hope (Fig. 2d).

### 3 3.1.2 Spatial extent of the aerosol plume

4 The transport of the volcanic aerosol plume over the southern hemisphere can be followed by  
5 CALIOP observations at 532 nm. Figure 3 shows the CALIOP cross-section of the 532nm total  
6 attenuated backscatter (TAB) for the overpass over South America on 24 April. The TAB  
7 signals ranging from  $1 \cdot 10^{-3}$  to  $5 \cdot 10^{-3} \text{ km}^{-1} \text{ sr}^{-1}$  corresponding to weak values of brightness  
8 temperatures over the southern part of Brazil ( $34.22^\circ\text{S}$ ;  $53.97^\circ\text{W}$ ) can be attributed to volcanic  
9 material injected up to the lower stratosphere by the Calbuco eruption. Figure 4 and 5 present  
10 the latitude-altitude cross sections of the scattering ratio observed by CALIOP for 16-day  
11 selected periods in 2015. The data displayed in Figure 4 and 5 correspond to the zonal mean  
12 averages of CALIOP scattering ratio during 16-day periods. The data are calculated within  $1^\circ$   
13 latitudinal zonal bands and have about 9% precision (Vernier et al., 2009). The scattering ratio  
14 values observed during the 16-30 April period (before the eruption) in the Southern hemisphere,  
15 particularly in the lower stratosphere, were in average at 1.05 (not shown). Between one and  
16 three weeks after the eruption (1-16 May period), CALIOP observations reveal that SR  
17 increased up to 1.12 in the southern lower stratosphere (Fig. 4a). The amplitude of the plume  
18 during the first weeks following the eruption was higher than the background aerosol levels at  
19 mid-latitudes but was still below the scattering ratio values observed in the tropics. The first  
20 weeks following the eruption correspond to the period when the  $\text{SO}_2$  is still being converted  
21 (Fig. 1). The elevated backscatter in the tropics could be attributed to possible remnants of the  
22 Kelud ( $7.5^\circ\text{S}$ ;  $112.2^\circ\text{E}$ ; erupted in February 2014) volcanic aerosol superimposed to the  
23 equatorial background aerosol layer (Kristiansen et al., 2015). About one month after the  
24 eruption (16-31 May period) the Calbuco plume was much more pronounced with scattering  
25 ratio values (ranging from 1.16 to 1.18) largely above values observed before the eruption from  
26 CALIOP and greater than aerosol amounts confined in the tropical reservoir (Fig. 4b). The  
27 second half of May (16-31 May) corresponds to the period where the  $\text{SO}_2$  has been oxidized to  
28 aerosol. The plume extended up to about 20 km in altitude and spread over a wide range of  
29 latitudes, nearly reaching  $60^\circ\text{S}$  and intruding into low latitudes near  $5^\circ\text{S}$ . About one month later  
30 (16-30 June), the plume top had moved upward by several hundred meters and the layer was  
31 thicker (Fig. 5a). The southern hemisphere between  $10^\circ\text{S}$  and polar latitudes was full of volcanic  
32 aerosol with scattering ratio values much higher than elsewhere in the whole stratosphere.  
33 About four months after the eruption (16-31 August) the volcanic aerosol layer was even thicker

1 with scattering ratio remaining high (Fig. 5b). Figure 5d also reveals a deepening of the volcanic  
2 aerosol layer and an enhancement of the equatorial backscatter in the Upper Troposphere.  
3 In the 21-28 km altitude range, detrainment of aerosol from the equatorial reservoir depends  
4 upon the phase of the quasi-biennial oscillation (QBO) and on the intensity of planetary wave  
5 activity (Trepte and Hitchman, 1992). Through the use of numerical model, Pitari et al (2016b)  
6 discussed on the impact of the QBO phase on the meridional transport of the aerosols plume to  
7 mid- and high latitudes. They revealed that the volcanic aerosols is confined to the tropics when  
8 the volcanic eruption occurred during the easterly shear of the QBO. When QBO easterlies  
9 descend in the tropics, propagation of planetary waves is inhibited from entering this region,  
10 thus limiting the extent to which these waves may detrain aerosol laterally from the tropical  
11 reservoir (Trepte et al., 1993). This corresponds to the situation in April-May, 2015 (Figure 4a,  
12 b). However, during the westerly phase of the QBO, mixing across the subtropics is favored,  
13 especially in winter (Trepte et al., 1993). The meridional spread in aerosols to southern  
14 midlatitudes shown above 21 km in Figure 5a and 5d is consistent with the phase reversal of  
15 the QBO from easterlies to westerlies observed from mid-2015.

## 16 **3.2 Evolution of the aerosols plume over the Reunion site**

### 17 **3.2.1 Ground-based and satellite observations**

18 Figure 6 depicts the evolution of the stratospheric AOD (sAOD) at 532 nm calculated between  
19 17 and 30 km from the Reunion ground-based LiDAR and OMPS observations over Reunion  
20 Island from November 2014 to November 2016. The wavelength conversions to 532 nm were  
21 performed using the Angström exponents where detailed description of the methodology is  
22 given by Khaykin et al (2017). The Angström exponents for the 355-532 nm and 532-675 nm  
23 pairs were adopted from Jäger and Deshler (2002) and Khaykin et al (2017) set to -1.3 and -1.8  
24 respectively. sAOD were calculated from LiDAR and OMPS observations at 532 nm using  
25 Angstrom exponent mentioned previously. As expected, an increase in the aerosol loading was  
26 observed over the Reunion site a few weeks after the Calbuco eruption. OMPS data show a  
27 doubling in the sAOD record in comparison with values observed at the end of 2014 and at the  
28 beginning of 2015 (Fig. 6). sAOD reached its maximum values (0.014 for OMPS) at the  
29 beginning of June 2015, decreased afterward to 0.01 on August 2015 and went back to pre-  
30 eruption values (0.004-0.006) in April 2016. The LiDAR record peaks at the same period, but  
31 sAOD values are 1.2 times weaker than those observed by OMPS during the June-December  
32 period. The lidar sAOD observations show less difference with values obtained prior to the

1 eruption (0.008). Discrepancies between OMPS and LiDAR were significantly reduced by  
2 April 2016, (cf. relative differences of 25% over the January-December 2015 period and 10%  
3 over the April-November 2016 period). From both datasets an aerosol e-folding of  
4 approximately 90 days can be derived, which is rather close to the value (~80 days) reported  
5 for the Sarychev eruption (Jégou et al., 2013).

6 Figure 7a illustrates the weekly-averaged extinction profiles at 532 nm derived from LiDAR  
7 measurements over Reunion Island. This figure reveals a sharp increase of the extinction  
8 between 18 and 19 km in May 2015 and reaching its maximum value (greater than  $4 \times 10^{-3} \text{ km}^{-1}$ )  
9 in June. The vertical extent of the plume had increased significantly over the May-July period  
10 with a volcanic aerosol layer spanning from 18 to 21 km. At the beginning of June, the plume  
11 was structured in two layers with the first one centered at 18.5 km and the second one at 20 km  
12 (Fig.7a). We note also a brief decrease in the local extinction, ranging from  $1.5$  to  $3 \text{ km}^{-1}$ , around  
13 mid-May. The variability observed in the weekly-averaged extinction profiles and in the  
14 vertical extent of the aerosol signal over the May-July period reflects the presence of transient  
15 aerosol layers above Reunion Island and indicates that the plume is not homogeneously  
16 distributed at this stage. The altitude of the volcanic aerosol plume and the extinction values  
17 decreased from mid-August onwards. The plume is hence centered around 18 km in September,  
18 and extinction values in September are around two times less than those observed in June. This  
19 decrease of the extinction values is accompanied by a decrease of the altitude of the plume and  
20 could be due to the sedimentation processes (Fig. 7a). Hamil et al (1997) revealed that  
21 sedimentation can play a significant role in loss of stratospheric aerosol to the troposphere.

22 Overall, the temporal evolution of the weekly-averaged extinction presents similar general  
23 features as the LiDAR observations, with maximum values in June and a subsequent gradual  
24 decrease of the aerosol signal. Nevertheless, in the OMPS data the plume is smeared out over  
25 a wider vertical range than in the lidar record (Fig. 7b). The vertical and horizontal structures  
26 of the plume are not reproduced in the OMPS data. In particular, the decrease in the plume  
27 altitude in mid-August is not observed by OMPS. More generally, extinction values observed  
28 by OMPS in the 15-17 km altitude range are higher than those observed by the LiDAR. The  
29 evolution of the scattering ratio at 532 nm obtained from the LiDAR and CALIOP space-borne  
30 observations during the April-December 2015 period over the Reunion Island site are presented  
31 on Figure 8. The scattering ratios from CALIOP have been averaged within  $\pm 5^\circ$  in latitude and  
32  $\pm 50^\circ$  in longitude (extending from Africa to Australia) around Reunion Island (Fig. 8b).  
33 CALIOP observations confirm the presence of the volcanic aerosol plume over the Reunion

1 Island site at the beginning of May 2015 with maximum scattering ratio values (greater than  
2 1.9) on mid-May 2015. Overall, the aerosol variability is smoother in CALIOP observations  
3 than in the LiDAR record, which shows more fluctuations in the altitude of the volcanic plume.  
4 In contrast to the LiDAR and OMPS observations, CALIOP data do not show an increase in  
5 the vertical extent of the plume and maximum scattering ratio values at the beginning of June  
6 2015. According to CALIOP, the scattering ratio begins to decrease in mid-June followed by a  
7 slight decrease of the altitude of the plume from the end of July (Fig 8b). From July onwards,  
8 the CALIOP aerosol scattering ratios decrease gradually with similar values as observed by the  
9 LiDAR. The decrease of the aerosol scattering ratio is associated with a descent in the altitude  
10 of the plume, which could be due to sedimentation, and is consistent with the observations from  
11 OMPS.

12 The reasons for these discrepancies between ground-based and satellite observations may be  
13 multiple but effects due to different spatial samplings cannot be excluded. The difference in  
14 vertical resolution between ground-based LiDAR and satellites (OMPS, CALIOP) which could  
15 be one possible cause at the origin of discrepancies. The discrepancies between the satellites  
16 and ground-based LiDAR could be significant when the difference of vertical resolution is high  
17 between these devices. We note that the vertical resolution of OMPS is 10 times lower than the  
18 ground-based LiDAR with 0.15 km and 1.5 km respectively (Jaross et al., 2014). Thus, the  
19 structures of the plume look smoother than those obtained from the ground-based LiDAR. In  
20 the case of CALIOP where the vertical resolution is better (~ 3 times less to the ground-based  
21 LiDAR), the differences in the structure of the plume are less. Moreover, the discrepancies  
22 existing between results presented in this study could be also due to horizontal resolution or  
23 different measurement techniques. Unlike satellite experiments that allow global observations,  
24 a ground-based LiDAR system is able to derive aerosols characteristics at a specific location.  
25 OMPS views the Earth's limb looking backward along the orbit track of approximately 125 km  
26 with a horizontal resolution of 50 km. It is difficult for OMPS to detect with accuracy small  
27 amount of aerosol at a local point with these weak vertical and horizontal resolutions. It is for  
28 this reason that the structure of the plume observed since July is not in agreement with the  
29 ground-based LiDAR. Given that the weak horizontal resolution of CALIOP (500 km) (Vernier  
30 et al., 2011), it is consistent to observe weaker values than the ground-based LiDAR. As we  
31 will discuss more details in Section 4, the dynamical context can induce an inhomogeneity of  
32 the plume. As a consequence, this inhomogeneity of the plume could lead to incorrect  
33 identification of the volcanic aerosols by the satellites. Vernier et al. (2011) reported that it is

1 possible for solid aerosols such ash ash to be incorrectly identified as “ice nuclei” and to be  
2 then removed.

### 3 **3.2.2 In-situ observations**

4 Four LOAC OPCs were launched over the Reunion Island site on 26 November 2014, 19 May  
5 2015, 19 August 2015, and 2 November 2016 respectively. sAOD 532 nm were calculated  
6 following Mie Theory from fits to the observed size distributions at each level. LOAC  
7 observations also reveal an increase by a factor of 2 in the sAOD on 19 May 2015 ( $1.35 \times 10^{-2}$ )  
8  $^2$ ). sAOD decreases to  $8.4 \times 10^{-3}$  on 19 August 2015 followed by a return to pre-eruption levels  
9 by November 2016 (Fig. 6). The overall evolution of sAOD derived from LOAC compares  
10 fairly well to OMPS and to lidar observations, accounting for error bars (Fig. 6). The 10-second  
11 sampling rate of the LOAC instrument and the ascent velocity of the balloon determine the  
12 vertical resolution. The difference observed between the daily-integrated LiDAR and the in-  
13 situ data may be due to the 1-minute averaging of the in-situ data, which tends to smooth  
14 structure attributed to the volcanic aerosols.

15 Figure 9 illustrates the number ( $dN/d\ln(D)$ ) and volume ( $DV/d\ln(D)$ ) concentrations obtained  
16 from the LOAC OPC observations over the Reunion Island site on 19 May 2015 at 1746 UTC.  
17 LOAC OPC observations reveal a size distribution with decreasing concentrations for particle  
18 sizes larger than  $0.2 \mu\text{m}$  (Fig. 9). The value of  $0.2 \mu\text{m}$  represents the lower bound of the LOAC  
19 size range, so the data may miss possible secondary modes for smaller particles (Wilson et al.,  
20 2008). Particle concentrations for sizes larger than  $1 \mu\text{m}$  too low to properly detected by the  
21 LOAC OPC but undoubtedly indicate a coarse mode. However there is no clear evidence for a  
22 bimodal distribution, as observed during the first weeks after the eruption of Mt. Pinatubo, an  
23 intense second mode possibly consisting of volcanic ash (e.g. Russell et al., 1996). The shape  
24 of the size distribution obtained during the Calbuco event is similar to that obtained by Kravitz  
25 et al. (2011) for the Sarychev eruption. As suggested by Kravitz et al. (2011), we can also  
26 assume that the Calbuco eruption did not eject enough material to create a bimodal structure  
27 over Reunion Island.

28 The effective radius derived from the LOAC OPC on 19 May is  $0.17 \pm 0.02 \mu\text{m}$  indicating that  
29 the particles observed several weeks after the Calbuco eruption are quite small. Interestingly,  
30 Jégou et al. (2013) reported that the effective radius obtained during the Sarychev event ranged  
31 from  $0.15$  to  $0.20 \mu\text{m}$  more than one month after the eruption, in agreement with the results of  
32 O’Neill et al. (2012). Therefore, both eruptions are comparable in terms of size distribution  
33 shape and effective radius. Russell et al. (1996) reported that in the month following the

1 Pinatubo eruption the mean effective radius did not differ greatly from pre-eruption values (i.e.  
2  $0.17 \pm 0.07 \mu\text{m}$  in their study), possibly because a large number of particles with sizes both  
3 smaller and larger than  $0.17 \mu\text{m}$  were injected (the latter consisting most likely of volcanic ash).  
4 Russell et al (1996) discussed how particle growth processes (condensation and coagulation),  
5 may be compensated by particle loss, which tends to decrease mean effective radius. This could  
6 explain the weak evolution on the effective radius during the month following the Pinatubo  
7 eruption.

8 The integrated number of particles obtained over the full 19 size classes from 0.2 to  $2 \mu\text{m}$  in  
9 diameter is presented in Figure 10. A local aerosol concentration enhancement is detected in  
10 the lower stratosphere (16.8-19 km) over Reunion Island on 19 May 2015 at 1746 UTC. A  
11 maximum concentration of about 150 particles per  $\text{cm}^3$  (total number of particles:  $730 \pm 130$   
12 particles ( $\pm 1\sigma$ )) is observed by the aerosol counter for particle sizes larger than  $0.2 \mu\text{m}$ . Few in  
13 situ observations are available in the tropical region such as Reunion Island to provide a  
14 reference state of the background aerosol content. In comparison to LOAC flight on 26  
15 November 2014 at 1442 UTC (five months before the eruption), the aerosol number  
16 concentration observed on 19 May 2015 is  $\sim 20$  times higher. Three months later, another LOAC  
17 OPC was launched over the Reunion Island site but the in situ profile only partially shows the  
18 volcanic aerosol layer because of a telemetry loss. The aerosol number concentration obtained  
19 on 19 August 2015 at 1300 UTC over Reunion Island may reveal a tendency to return to  
20 concentration values observed before the eruption (Fig. 10), with a number concentration of 40  
21 particles per  $\text{cm}^3$  in the lower stratosphere. This tendency is confirmed with the LOAC flight  
22 conducted on 2 November 2016 at 2030 UTC with a total number concentration close to 20  
23 particles per  $\text{cm}^3$  in the lower stratosphere (Fig. 10).

24 The residence time of the aerosol particles in the stratosphere depends on the balance between  
25 the growth processes and the removal processes which are likely to be controlled by the  
26 dynamical context. In the following section, we will discuss the influence of the dynamical  
27 activity on the variability of the volcanic aerosol over the southern hemisphere.

## 28 **4. Dynamical modulation of the aerosol plume**

### 29 **4.1 Long-range transport**

30 In order to analyze the isentropic transport, the high resolution MIMOSA model has been used  
31 to produce a continuous evolution of PV fields for the period from 1 April 2015 to 31 August  
32 2015. Four advected PV maps, derived for the 400 K isentropic level from the MIMOSA model,



1 together with dynamical barrier locations derived from the DyBaL code are superimposed in  
2 Figures 11 and 12. The localization of the volcanic aerosol plume obtained from OMPS  
3 observations at  $400 \text{ K} \pm 5 \text{ K}$  isentropic level is also superimposed (Fig. 11 and 12). On 24 April  
4 2015, a significant wave activity is observed, leading to a fairly mixed surf zone in the  $20^\circ\text{S}$ -  
5  $60^\circ\text{S}$  latitude band (not shown). The Calbuco plume is situated inside the surf zone and the  
6 plume was mixed equatorward. On 27 April 2015, the subtropical and mid-latitude barrier are  
7 detected following the Nakamura's formalism (described in Section 2.3) around  $15^\circ\text{S}$  (red line,  
8 Fig. 11) and  $40^\circ\text{S}$  (blue line) in latitude respectively, limiting the geographical extent of the  
9 plume (Fig. 11a). **Figure 11a shows clearly that the air masses containing aerosols cannot move**  
10 **beyond the south of Brazil because of the presence of the subtropical barrier.** On 01 May 2015,  
11 the air masses were confined between the two dynamical barriers located in average at  $25^\circ\text{S}$   
12 (red line, Fig. 11b) and  $40^\circ\text{S}$  (blue line, Fig. 11b) in latitude respectively. The air masses were  
13 advected eastward between South Africa and Madagascar following the wave shape of the  
14 barrier, consistent with the OMPS observations near South Africa (Fig. 11b). The subtropical  
15 barrier previously located at  $25^\circ\text{S}$  (red line, Fig. 11b) moved northward crossing South Africa.  
16 The air masses containing aerosol previously situated in the south side of Madagascar were  
17 transported northward and eastward following the displacement of the barrier and reached the  
18 Reunion Island site.

19 On 19 May 2015 (Fig. 12a), the volcanic aerosol plume was confined between the two  
20 dynamical barriers and advected eastward. At this stage, the presence of the subtropical barrier  
21 and the polar vortex seems to constrain the Calbuco plume inducing its transport eastward.  
22 Between end of May and beginning of June, the subtropical barrier has dissipated while the  
23 edge of the polar vortex was around  $\sim 40^\circ\text{S}$  (blue line, Fig. 12b). The OMPS observations reveal  
24 that the most part of the plume was located over the southern African and the Indian Ocean  
25 region in June (Fig. 12b). On the following months of July and August, the polar vortex is  
26 clearly identified at  $60^\circ\text{S}$  (blue line, Fig. 12b) which is a classical pattern for the austral winter.

27 **This present study discuss only on the transport of the volcanic aerosols plume at 400 K**  
28 **isentropic level (isentropic level where the Calbuco plume is detected at Reunion). Figure 4 and**  
29 **5 reveal that the meridional transport of the plume occurred between 12 and 20 km. As a**  
30 **consequence, the transport of the Calbuco plume at another isentropic level associate to another**  
31 **pathways described above is possible. Figure 5b reveals also the possibility to the Calbuco**  
32 **aerosols plume to penetrate the polar vortex at the end of August 2015. This assumption seems**  
33 **to be consistent to the works reported by Ivy et al. (2017) and Solomon et al. (2016). Based on**

1 SD-WACCM (Specified Dynamics-Whole Atmosphere Community Climate Model) model  
2 and balloon observations at Syowa (69°S; 34.58°E), Solomon et al. (2016) discussed on the  
3 impact of the Calbuco plume on the deepest Antarctic ozone depletion observed in October  
4 2015. They reveal that the integrated additional Antarctic ozone column losses averaged over  
5 the polar cap are between 5 and 13 DU following the Calbuco eruption. Through the use of FR-  
6 WACCM (free-running Whole Atmosphere Community Climate Model), Ivy et al. (2017)  
7 shown that the forced response to the eruption of Calbuco was an increase in the size of the  
8 ozone hole by  $4.5 \cdot 10^6 \text{ km}^2$ .

## 9 **4.2 Removal processes**

10 As discussed above, in the lower stratosphere distributions of the aerosol are modulated (or  
11 mostly driven) by isentropic transport. However, particle removal processes should be  
12 considered. As reported by Kremser et al (2016), aerosol in the vicinity of the tropopause can  
13 be transported into the troposphere by variety of mechanisms. Hamill et al. (1997) reported that  
14 stratosphere-troposphere exchange (STE) on isentropic surfaces due to Rossby wave activity  
15 can be considered a significant dynamical process for removal of stratospheric aerosol.  
16 Depending on the strength of the Brewer-Dobson circulation, stratospheric materials such as  
17 aerosols can be rapidly transported from the tropics to high latitudes (Dhomse et al., 2006,  
18 2014). Based on semi-Lagrangian and analyzed winds from ECMWF, Chen et al. (1995)  
19 investigated the extratropical STE on isentropic surfaces that intersect the tropopause. Above  
20 340 K they found that STE exhibits a strong annual cycle where very little STE takes place in  
21 the winter hemisphere, but significant STE occurs in the summer hemisphere, particularly in  
22 the northern summer. The weak STE in the winter hemisphere is mainly due to the barrier effect  
23 of the strong PV gradient at the tropopause (Chen et al., 1995). Through the use of 10 years of  
24 LiDAR observations at Pasadena (34°N, 118°W; California), Menzies and Tratt. (1995) found  
25 a clear link between the aerosol optical properties in UT-LS and the active extratropical STE  
26 processes occurring the winter and early spring. The calculated stratospheric mass extrusion  
27 rate is consistent with a 45-day lifetime of lower stratospheric aerosol during this part of the  
28 year, which implies that extratropical STE is a significant sink for stratospheric aerosol  
29 (Menzies and Tratt, 1995). Given the potential of a STE event to impact the stratospheric  
30 aerosol loading, we cannot exclude its contribution (even though small) on the stratospheric  
31 aerosols loading at Reunion Island.

32 Dhomse et al. (2014) using the CCM model (UM-UKCA) discussed the influence of STE  
33 events on the budget of the stratospheric aerosol. In particular, they suggested that a general

1 overestimation of STE in global composition climate models could lead to overestimated  
2 removal of aerosols from stratosphere into the troposphere. Through the use of ULAQ-CCM  
3 model, Pitari et al (2016b) shown that the efficiency of STE depends on large-scale transport  
4 following the down-welling branch of the Brewer-Dobson circulation together with  
5 gravitational settling. The long-range transport of a volcanic plume is less likely to be  
6 isentropic, due to sedimentation of ash or other large particles (with any accommodated  
7 sulphur) within the plume. The modulation of the plume over Reunion Island could be caused  
8 by particle removal processes such sedimentation (considered as the primary loss mechanism  
9 of stratospheric aerosol) or by dilution of the stratospheric plume (Hamill et al, 1997; Rasch et  
10 al., 2008). Sedimentation is an effective removal mechanism for particles that survive long  
11 enough in the stratosphere to grow to larger sizes (Hamill et al., 1997).

12 We note the potential role of removal processes on the initial dispersion of volcanic aerosols,  
13 in particular co-emitted ultrafine ash particles, but do not explore this effect here. Highlighting  
14 removal processes from Figures 7 and 8 is somewhat complicated by the transience in plume  
15 altitudes especially in the LiDAR local data. The potential role of removal processes on the  
16 evolution of the plume requires further investigation and will form the basis for a forthcoming  
17 study.

## 18 **5. Summary and conclusion**

19 The long-range transport of the volcanic aerosol produced following the Calbuco eruption has  
20 been examined. The analysis focuses on the dynamical context which led to the spread of the  
21 aerosol plume over Indian Ocean between April 2015 and November 2016. The transport of the  
22 volcanic aerosols to the Indian Ocean was investigated by combining satellite (CALIOP, IASI,  
23 OMPS), and ground-based experiments: Optical Particle Counter (LOAC) and lidar, in addition  
24 to numerical tools: the DyBal code and the high-resolution MIMOSA model.

25 The amount of SO<sub>2</sub> injected into the atmosphere during the Calbuco eruption has been  
26 quantified using IASI observations. SO<sub>2</sub> mass emitted by the Calbuco eruption was about two  
27 times lower than for the moderate northern hemisphere eruption of Sarychev in June 2009, but  
28 had a similar SO<sub>2</sub> e-folding time (Jégou et al., 2013; Kravitz et al., 2011). It is found from  
29 CALIOP observations that the Calbuco aerosol layer was observable in the lower stratosphere,  
30 between 18 and 21 km, and spread exclusively in the southern hemisphere. OMPS observations  
31 reveal that the Calbuco plume reached the Indian Ocean two weeks after the eruption. It is  
32 shown from ground-based observations deployed at Reunion Island that SAOD increased by a  
33 factor of ~2 by the beginning of May 2015 and decreased afterward, returning to pre-eruption

1 values by November 2016. The aerosol e-folding time is estimated to be ~90 days, close to the  
2 ~80 days reported for the Sarychev eruption (Jégou et al., 2013). Though the various datasets  
3 agree in terms of aerosol signal intensity, we report significant differences for the plume height  
4 and its variability, possibly as a result of different observations geometries, resolutions and  
5 spatial scales inherent to each instrument.

6 In situ measurements by the LOAC OPC have pointed out the impact of the Calbuco eruption  
7 on the lower stratospheric aerosol content over the Reunion Island site. Aerosol number  
8 concentrations were 20 times higher than values observed before and one year after the  
9 eruption. On May 2015, the volcanic aerosol was characterized by an effective radius of  $0.16$   
10  $\pm 0.02$   $\mu\text{m}$  and a unimodal lognormal size distribution above 250 nm diameter. These  
11 microphysical characteristics are in agreement with previous studies focusing on the Sarychev  
12 eruption (Kravitz et al., 2011; Jégou et al., 2013).

13 Through the use of the MIMOSA model and the DyBAL code, it was clearly identified that the  
14 eastward transport of the volcanic aerosols occurred mainly in form of planetary-scale tongues.  
15 In particular, the combination of MIMOSA and DyBal simulations revealed that the transport  
16 of the volcanic aerosol plume eastward was confined between subtropical barrier and mid-  
17 latitude (polar vortex) dynamical barriers, within which most of the zonal transport took place.  
18 Our results support the assumption that the processes explaining the structure of the plume over  
19 the southern hemisphere had mainly a dynamical origin. Thus, the fluctuation of the subtropical  
20 barrier induced transient aerosol layers above Reunion Island and an inhomogeneous  
21 distribution of the plume between May and July 2015. The present study also supports the  
22 hypothesis that the modulation of a volcanic plume results from a contribution of both  
23 dynamical and microphysical processes. Fully understanding the contribution of the  
24 microphysical processes to the evolution of the volcanic plume over the southern hemisphere  
25 requires further investigation. This will be examined in a forthcoming study.

26

1 **Acknowledgements**

2 This work is supported by the Labex « Étude des géofluides et des VOLatils–Terre, Atmosphère  
3 et Interfaces - Ressources et Environnement (VOLTAIRE) (ANR-10-LABX-100-01). This  
4 study is integrated and supported by the LEFE project SATORI (Stratospheric Aerosols in the  
5 Tropic Observed from Reunion Island). The authors thank the LPC2E and UMS balloon  
6 launching team for their technical collaboration. We would especially like to thank the staff of the  
7 team working on the lidar systems at the Maïdo observatory. Lieven Clarisse is a research associate with  
8 the Belgian FNRS-F.R.S. The authors thank also the CALIOP team and Jean-Paul Vernier for  
9 processing and providing data. We are also grateful to the CCUR team for the use of the TITAN  
10 supercomputer. We thank also Duncan Fairlie for his contribution to check and improve the  
11 English of this paper.

12

## 1 **References**

- 2 Arfeuille, F., B. P. Luo, P. Heckendorn, D. Weisenstein, J. X. Sheng, E. Rozanov, M. Schraner,  
3 S. Brönnimann, L.W. Thomason, and T. Peter: Modeling the stratospheric warming following  
4 the Mt. Pinatubo eruption: uncertainties in aerosol extinctions, *Atmos. Chem. Phys.*, 13, 11221–  
5 11234, 2013.
- 6 Baray, J. L., Courcoux, Y., Keckhut, P., Portafaix, T., Tulet, P., Cammas, J. P., ... & Desmet,  
7 F. (2013). Maïdo observatory: a new high-altitude station facility at Reunion Island (21° S, 55°  
8 E) for long-term atmospheric remote sensing and in situ measurements. *Atmospheric*  
9 *Measurement Techniques*, 6(10), 2865-2877.
- 10 Bauman, J. J., Russell, P. B., Geller, M. A. and Hamill, P. : A stratospheric aerosol climatology  
11 from SAGE II and CLAES measurements: 2. Results and comparisons, 1984–1999. *J.*  
12 *Geophys. Res.* 108, 4383. (doi:10.1029/2002JD002993, 2003
- 13 Bekki, S : On the possible role of aircraft-generated soot in the middle latitude ozone depletion,  
14 *J. Geophys. Res.*, 102, 10,751-10,758, 1997
- 15 Bencherif, H., Portafaix, T., Baray, J. L., Morel, B., Baldy, S., Leveau and J., Diab, R. : LIDAR  
16 observations of lower stratospheric aerosols over South Africa linked to large scale transport  
17 across the southern subtropical barrier. *Journal of atmospheric and solar-terrestrial physics*,  
18 65(6), 707-715, 2003
- 19 Bencherif, H., Amraoui, L. E., Semane, N., Massart, S., Charyulu, D. V., Hauchecorne, A., and  
20 Peuch, V. H., Examination of the 2002 major warming in the southern hemisphere using  
21 ground-based and Odin/SMR assimilated data: stratospheric ozone distributions and  
22 tropic/mid-latitude exchange. *Canadian Journal of Physics*, 85(11), 1287-1300, 2007
- 23 Bluth, G. J. S., Doiron, S. D., Schnetzler, C. C., Krueger, A. J., and Walter, L. S.: Global  
24 tracking of the SO<sub>2</sub> clouds from the June 1991 Mount Pinatubo eruptions, *Geophys. Res. Lett.*,  
25 19, 151–154, doi:10.1029/91GL02792, 1992.
- 26 Borrmann, S., Solomon, S., Dye, J. E., Baumgardner, D., Kelly, K.K., and Chan, K. R. :  
27 Heterogeneous reactions on stratospheric background aerosols, volcanic sulfuric acid droplets,  
28 and type I PSCs: The effects of temperature fluctuations and differences in particle phase, *J.*  
29 *Geophys. Res.*, 102, 3639–3648, 1997.

1 Bourassa, A. E., D. A. Degenstein, B. J. Elash, and E. J. Llewellyn : Evolution of the  
2 stratospheric aerosol enhancement following the eruptions of Okmok and Kasatochi: Odin-  
3 OSIRIS measurements, *J. Geophys.Res.*, 115, D00L03, doi:10.1029/2009JD013274, 2010

4 Bourassa, A. E., McLinden, C. A., Bathgate, A. F., Elash, B. J., and Degenstein, D. A.: Precision  
5 estimate for Odin-OSIRIS limb scatter retrievals, *J. Geophys. Res.*, 117, D04303,  
6 doi:10.1029/2011JD016976, 2012

7 Canty, T., Mascioli, N. R., Smarte, M. D., & Salawitch, R. J. (2013). An empirical model of  
8 global climate-Part 1: A critical evaluation of volcanic cooling. *Atmospheric Chemistry and*  
9 *Physics*, 13(8), 3997.

10 Carn, S., L. Clarisse, and A. J. Prata : Multi-decadal satellite measurements of global  
11 volcanic degassing, *J. Volcanol. Geotherm. Res.*, 99-134, 2016

12 Chen, P., J. R. Holton, A. O'Neill, and R. Swinbank : Isentropic mass exchange between the  
13 Tropics and extratropics in the stratosphere. *J. Atmos. Sci.*, **51**, 3006–3018, 1994

14 **Chen, P: Isentropic cross-tropopause mass exchange in the extratropics. *Journal of Geophysical***  
15 ***Research: Atmospheres*, 100(D8), 16661-16673, 1995**

16 Clarisse, L., Coheur, P. F., Prata, A. J., Hurtmans, D., Razavi, A., Phulpin, T., Hadji-Lazaro, J.,  
17 and Clerbaux, C.: Tracking and quantifying volcanic SO<sub>2</sub> with IASI, the September 2007  
18 eruption at Jebel at Tair, *Atmos. Chem. Phys.*, 8, 7723-7734, doi:10.5194/acp-8-7723-2008,  
19 2008.

20 Clarisse, L., Hurtmans, D., Clerbaux, C., Hadji-Lazaro, J., Ngadi, Y., and Coheur, P.-F.:  
21 Retrieval of sulphur dioxide from the infrared atmospheric sounding interferometer (IASI),  
22 *Atmos. Meas. Tech.*, 5, 581–594, doi:10.5194/amt-5-581-2012, 2012.

23 Clarisse, L., Coheur, P. F., Theys, N., Hurtmans, D. and Clerbaux, C.: The 2011 Nabro eruption,  
24 a SO<sub>2</sub> plume height analysis using IASI measurements. *Atmospheric chemistry and physics*,  
25 *14*(6), 3095-3111, 2014

26 Clerbaux, C., Boynard, A., Clarisse, L., George, M., Hadji-Lazaro, J., Herbin, H. and Wespes,  
27 C. Monitoring of atmospheric composition using the thermal infrared IASI/MetOp sounder.  
28 *Atmospheric Chemistry and Physics*, 9(16), 6041-6054, 2009

1 Dhomse, S., Weber, M., Wohltmann, I., Rex, M., and Burrows, J. P., On the possible causes of  
2 recent increases in northern hemispheric total ozone from a statistical analysis of satellite data  
3 from 1979 to 2003. *Atmospheric Chemistry and Physics*, 6(5), 1165-1180, 2006

4 Dhomse, S. S., Emmerson, K. M., Mann, G. W., Bellouin, N., Carslaw, K. S., Chipperfield, M.  
5 P. and Dalvi, M. , Aerosol microphysics simulations of the Mt.~ Pinatubo eruption with the  
6 UM-UKCA composition-climate model. *Atmospheric Chemistry and Physics*, 14(20), 11221-  
7 11246, 2014

8 Fairlie, T. D., J. P. Vernier, M. Natarajan, and K. M. Bedka (2014), Dispersion of the Nabro  
9 volcanic plume and its relation to the Asian summer monsoon, *Atmos. Chem. Phys.*, 14(13),  
10 7045-7057, doi:10.5194/acp-14-7045-2014.

11 Froyd, K. D., D. M. Murphy, T. J. Sanford, D. S. Thomson, J. C. Wilson, L. Pfister, and L. Lait  
12 : Aerosol composition of the tropical upper troposphere, *Atmos. Chem. Phys.*, 9, 4363-4385,  
13 2009

14 Fussen, D., F. Vanhellemont and C. Bingen, Evidence of transport, sedimentation and  
15 coagulation mechanisms in the relaxation of post-volcanic stratospheric aerosols, *Ann.*  
16 *Geophys.*, 19, 1157-1162, 2001

17 Godin, S., M. Marchand, and A. Hauchecorne, Influence of Arctic polar ozone depletion on the  
18 lower stratospheric ozone amounts at Haute-Provence Observatory (44° N, 60° E), *J. Geophys.*  
19 *Res*, 107(20), 10.1029/2001JD000516, 107(D20), 2002

20 Gorkavyi, N., D. F. Rault, P. A. Newman, A. M. d. Silva, and A. E. Dudorov : New stratospheric  
21 dust belt due to the Chelyabinsk bolide, *Geophys. Res. Lett.*, 40(17), 47284733,  
22 doi:10.1002/grl.50788, 2013

23 Grant, W. B., Browell, E. V., Fishman, J., Brackett, V. G., Veiga, R. E., Nganga, D., Long, C.  
24 S. : Aerosol-associated changes in tropical stratospheric ozone following the eruption of Mount  
25 Pinatubo. *Journal of Geophysical Research: Atmospheres*, 99(D4), 8197-8211, 1994

26 Grant, W. B., E. V. Browell, C. S. Long, L. L. Stowe, R. G. Grainger, and A. Lambert : Use of  
27 volcanic aerosols to study the tropical stratospheric reservoir. *J. Geophys. Res.*, **101**, 3973–  
28 3988, 1996

29 Hamill, P., Jensen, E. J., Russell, P. B., and Bauman, J.J.: The life cycle of stratospheric aerosol  
30 particles, *B. Am. Meteorol. Soc.*, 78, 1395–1410, doi:10.1175/1520-0477(1997)078, 2.0.CO;2,  
31 1997.



1 Hauchecorne, A.: Ether, Service Arletty, Atmospheric Model Description, ETH-ACR-AR-  
2 DM-001, 22 p., 1998.

3 Hauchecorne, A., Godin, S., Marchand, M., Heese, B., and Souprayan, C. Quantification of the  
4 transport of chemical constituents from the polar vortex to midlatitudes in the lower  
5 stratosphere using the high-resolution advection model MIMOSA and effective diffusivity.  
6 *Journal of Geophysical Research: Atmospheres*, 107(D20), 2002

7 Heese, B., Godin, S and Hauchecorne, A : Airborne lidar measurements of ozone filaments  
8 during METRO–A validation of PV advection model MIMOSA. *J. Geophys. Res*, 106, 20-011,  
9 2001

10 Hermann, M., J. Heintzenberg, A. Wiedensohler, A. Zahn, G. Heinrich, and C. A. M.  
11 Brenninkmeijer, Meridional distributions of aerosol particle number concentrations in the upper  
12 troposphere and lower stratosphere obtained by Civil Aircraft for Regular Investigation of the  
13 Atmosphere Based on an Instrument Container (CARIBIC) flights, *J. Geophys. Res.*, 108(D3),  
14 4114, doi:10.1029/2001JD001077, 2003.

15 Hitchman, M. H., M. McKay and C. R. Trepte (1994), A climatology of stratospheric aerosol,  
16 *J. Geophys. Res.*, 99, 20,689-20,700.

17 Hofmann, D., Barnes, J., O’Neill, M., Trudeau, M., and Neely, R.:Increase in background  
18 stratospheric aerosol observed with lidar at Mauna Loa Observatory and Boulder, Colorado,  
19 *Geophys. Res. Lett.*, 36, L15808, doi:10.1029/2009GL039008, 2009.

20 Hommel, R., Timmreck, C., Giorgetta, M. A. and Graf, H. F. (2015). Quasi-biennial oscillation  
21 of the tropical stratospheric aerosol layer. *Atmospheric Chemistry and Physics*, 15(10), 5557,  
22 2015

23 Jaross, G., Chen, G., Kowitt, M., Warner, J., Xu, P., Kelly, T. and Flittner, D : Suomi NPP  
24 OMPS Limb Profiler initial sensor performance assessment. In SPIE Asia-Pacific Remote  
25 Sensing (pp. 852805-852805), International Society for Optics and Photonics, 2012

26 Jumelet, J., S. Bekki, P. Seifert, N. Montoux, J.-P. Vernier, and J. Pelon (2009), Microphysical  
27 modeling of a midlatitude “polar stratospheric cloud” event: Comparisons against  
28 multiwavelength ground-based and spaceborne lidar data, *J. Geophys. Res.*, 114, D00H03,  
29 doi:10.1029/2009JD011776.

30 Junge, C. E., Chagnon, C. W. and Manson, J. E. (1961). Stratospheric aerosols. *Journal of*  
31 *Meteorology*, 18(1), 81-108.

1 Kinnison, D. E., K. E. Grant, P. S. Connell, D. A. Rotman, and D. J. Wuebbles (1994), The  
2 chemical and radiative effects of the Mount Pinatubo eruption, *J. Geophys. Res.*, 99(D12),  
3 25705–25731, doi:[10.1029/94JD02318](https://doi.org/10.1029/94JD02318).

4 Klett, J. D : Stable analytical inversion solution for processing lidar returns, *Appl. Opt.*, 20, 211  
5 – 220, 1981

6 Kravitz, B., Robock, A., and Bourassa, A.: Negligible climatic effects from the 2008 Okmok  
7 and Kasatochi volcanic eruptions, *J. Geophys. Res.*, 115, D00L05, oi:10.1029/2009JD013525,  
8 2010.

9 Kravitz, B., Robock, A., Bourassa, A., Deshler, T., Wu, D., Mattis, I., Finger, F., Hoffmann,  
10 A., Ritter, C., Bitar, L., Duck, T. J., and Barnes, J. E.: Simulation and observations of  
11 stratospheric aerosols from the 2009 Sarychev volcanic eruption, *J. Geophys. Res.*, 116,  
12 D18211, doi:10.1029/2010JD015501, 2011.

13 Kravitz, B., Robock, A., Shindell, D. T. and Miller, M. A.. Sensitivity of stratospheric  
14 geoengineering with black carbon to aerosol size and altitude of injection. *Journal of*  
15 *Geophysical Research: Atmospheres*, 117(D9), 2002

16 Kremser, S., Thomason, L. W., Hobe, M., *et al.* Stratospheric aerosol—Observations,  
17 processes, and impact on climate. *Reviews of Geophysics*, vol. 54, no 2, p. 278-335, 2016

18 Kristiansen, N. I., A. J. Prata, A. Stohl, and S. A. Carn : Stratospheric volcanic ash emissions  
19 from the 13 February 2014 Kelut eruption, *Geophys. Res. Lett.*, 42, 588–596,  
20 doi:10.1002/2014GL062307, 2015

21 Krotkov, N. A., M. R. Schoeberl, G. A. Morris, S. Carn, and K. Yang : Dispersion and lifetime  
22 of the SO<sub>2</sub> cloud from the August 2008 Kasatochi eruption, *J. Geophys. Res.*, 115,  
23 doi:10.1029/2010jd013984, 2010

24 Jäger, H., and T. Deshler, Lidar backscatter to extinction, mass and area conversions for  
25 stratospheric aerosols based on midlatitude balloonborne size distribution  
26 measurements, *Geophys. Res. Lett.*, 29(19), 1929, doi:10.1029/2002GL015609, 2002.

27 Jégou, F., Berthet, G., Brogniez, C., Renard, J. B., François, P., Haywood, J. M. and Godin-  
28 Beekmann, S. (2013). Stratospheric aerosols from the Sarychev volcano eruption in the 2009  
29 Arctic summer. *Atmospheric Chemistry and Physics*, 13(13), 6533-6552.

30 Labitzke, K. and McCormick, M.: Stratospheric temperature increases due to Pinatubo aerosols,  
31 *Geophys. Res. Lett.*, 19, 207–210, 1992.

1 Lurton, T., Renard, J.-B., Vignelles, D., Jeannot, M., Akiki, R., Mineau, J.-L. and Tonnelier,  
2 T.: Light scattering at small angles by atmospheric irregular particles: modelling and laboratory  
3 measurements, *Atmos., Meas. Tech.*, 7, 931-939, 2014.

4 McCormick, M. P., Thomason, L. W., and Trepte, C. R.: Atmospheric effects of the Mt  
5 Pinatubo eruption, *Nature*, 373, 399–404, 1995.

6 Menzies, R. T and Tratt, D. M.: Evidence of seasonally dependent stratosphere-troposphere  
7 exchange and purging of lower stratospheric aerosol from a multiyear lidar data set. *Journal of*  
8 *Geophysical Research: Atmospheres*, 100(D2), 3139-3148, 1995

9 Morel, B., Bencherif, H., Keckhut, P., Portafaix, T., Hauchecorne, A., and Baldy, S., Fine-scale  
10 study of a thick stratospheric ozone lamina at the edge of the southern subtropical barrier: 2.  
11 Numerical simulations with coupled dynamics models. *Journal of Geophysical Research:*  
12 *Atmospheres*, 110(D17), 2005

13 Nakamura, N., Two-dimensional mixing, edge formation, and permeability diagnosed in an  
14 area coordinate. *Journal of the atmospheric sciences*, 53(11), 1524-1537, 1996

15 Nair, P. J., Godin-Beekmann, S., Froidevaux, L., Flynn, L. E., Zawodny, J. M., Iii, J. R.  
16 and Leblanc, T : Relative drifts and stability of satellite and ground-based stratospheric ozone  
17 profiles at NDACC lidar stations. *Atmospheric Measurement Techniques*, 5(6063), 1301-1318,  
18 2012

19 Neely, R. R., P. Yu, K. H. Rosenlof, O. B. Toon, J. S. Daniel, S. Solomon, and H. L. Miller  
20 (2014), The contribution of anthropogenic SO<sub>2</sub> emissions to the Asian tropopause aerosol layer,  
21 *J. Geophys. Res.*, 119(3), 1571-1579, doi:10.1002/2013JD020578.

22 O'Neill, N. T., Perro, C., Saha, A., Lesins, G., Duck, T. J., Eloranta, E. W and Bourassa, A :  
23 Properties of Sarychev sulphate aerosols over the Arctic. *Journal of Geophysical Research:*  
24 *Atmospheres*, 117(D4), 2012

25 Portafaix, T., Morel, B., Bencherif, H., Baldy, S., Godin-Beekmann, S., and Hauchecorne, A..  
26 Fine-scale study of a thick stratospheric ozone lamina at the edge of the southern subtropical  
27 barrier. *Journal of Geophysical Research: Atmospheres*, 108(D6), 2003

28 Pueschel, R. F., Snetsinger, K. G., Russell, P. B., Kinne, S. A., & Livingston, J. M : The effects  
29 of the 1991 Pinatubo volcanic eruption on the optical and physical properties of stratospheric  
30 aerosols. *Proceedings of IRS92: Current Problems in Atmospheric Radiation*, 183-186, 1992

1 Rasch, P. J., Tilmes, S., Turco, R. P., Robock, A., Oman, L., Chen, C. C. J. and Garcia, R. R.,  
2 An overview of geoengineering of climate using stratospheric sulphate aerosols. *Philosophical*  
3 *Transactions of the Royal Society of London A: Mathematical, Physical and Engineering*  
4 *Sciences*, 366(1882), 4007-4037, 2008

5 Randel, W. J., Gille, J. C., Roche, A. E., Kumer, J. B., Mergenthaler, J. L., Waters, J. W. and  
6 Lahoz, W. A. (1993). Stratospheric transport from the tropics to middle latitudes by planetary-  
7 wave mixing. *Nature*, 365(6446), 533-535.

8 Rault, D.F and Loughmann,R.P : The OMPS Limb Profiler environmental data record  
9 algorithm theoretical basis document and expected performance, IEEE Transactions on  
10 Geoscience and Remote Sensing, 51(5), 2505-2527, 2013

11 Renard, J.B., Dulac, F., Berthet, G., Lurton, T., Vignelles, D., Jégou, F., Tonnelier, T., Thaury,  
12 C., Jeannot, M., Couté, B., Akiki, R., Verdier, N., Mallet, M., Gensdarnes, F., Charpentier, P.,  
13 Duverger, V., Dupont, J.V., Mesmin, S., Elias, T., Crenn, V., Sciare, J., Giacomoni, J., Gobbi,  
14 M., Hamonou, E., Olafsson, H., Dagsson-Waldhauserova, P., Camy-Peyret, C., Mazel, C.,  
15 Décamps, T., Piringer, M., Surcin, J., and Daugeron, D.: LOAC: a small aerosol optical  
16 counter/sizer for ground-based and balloon measurements of the size distribution and nature of  
17 atmospheric particles – Part 1: Principle of measurements and intercomparison campaigns,  
18 *Atmos. Meas. Tech.*, 9, 1721–1742, doi:10.5194/amt-9-1721-2016, 2016.

19 Ridley, D. A., et al. : Total volcanic stratospheric aerosol optical depths and implications for  
20 global climate change, *Geophys. Res. Lett.*, 41(22), 7763-7769, doi:10.1002/2014GL061541,  
21 2014

22 Russell, P. B., Livingston, J. M., Pueschel, R. F., Bauman, J. J., Pollack, J. B., Brooks, S. L.  
23 and Dutton, E. G. (1996). Global to microscale evolution of the Pinatubo volcanic aerosol  
24 derived from diverse measurements and analyses. *Journal of Geophysical Research:*  
25 *Atmospheres*, 101(D13), 18745-18763.

26 Sasano, Y., Browell, E. V. and Ismail, S : Error caused by using a constant  
27 extinction/backscattering ratio in the lidar solution. *Applied Optics*, 24(22), 3929-3932, 1985

28 Sawamura, P., Vernier, J. P., Barnes, J. E., Berkoff, T. A., Welton, E. J., Alados-Arboledas, L.  
29 and Lange, D. (2012). Stratospheric AOD after the 2011 eruption of Nabro volcano measured  
30 by lidars over the Northern Hemisphere. *Environmental Research Letters*, 7(3), 034013.

1 Siddaway, J. M., and S. V. Petelina (2010), Transport and evolution of the 2009 Australian  
2 Black Saturday bushfire smoke in the lower stratosphere observed by OSIRIS on Odin, J.  
3 Geophys. Res., 116, doi:10.1029/2010JD015162.

4 Solomon, S., Portmann, R. W., Garcia, R. R., Thomason, L. W., Poole, L. R., and McCormick,  
5 M. P.: The role of aerosol variations in anthropogenic ozone depletion at northern midlatitudes,  
6 J. Geophys. Res.-Atmos., 101, 6713–6727, 1996.

7 Solomon, S., Stratospheric ozone depletion: A review of concepts and history, Rev. Geophys.,  
8 37, 275–316, doi:10.1029/1999RG900008, 1999

9 Solomon, S., Daniel, J. S., Neely III, R. R., Vernier, J.-P., Dutton, E. G., and Thomason, L. W.:  
10 The persistently variable "Background" stratospheric aerosol layer and global climate  
11 change, Science 333, 866, doi:10.1126/science.1206027, 2011.

12 SPARC 2006 Assessment of stratospheric aerosol properties (ASAP). Technical report WCRP-  
13 124/WMO/TD-No. 1295/SPARC report no. 4, SPARC, Toronto, Ontario, CA, pp. 322.

14 Stenchikov, G. L., Kirchner, I., Robock, A., Graf, H. F., Antuna, J. C., Grainger, R. G., Lambert,  
15 A. and Thomason, L. 1998 Radiative forcing from the 1991 Mount Pinatubo volcanic eruption  
16 conditions. J. Geophys. Res. 103, 13 837–13 857. (doi:10.1029/98JD00693)

17 Stenchikov, G., A. Robock, V. Ramaswamy, M. D. Schwarzkopf, K. Hamilton, and S.  
18 Ramachandran, Arctic Oscillation response to the 1991 Mount Pinatubo eruption: Effects of  
19 volcanic aerosols and ozone depletion, J. Geophys. Res., 107(D24), 4803,  
20 doi:[10.1029/2002JD002090](https://doi.org/10.1029/2002JD002090), 2002.

21 Schuster, G. L., O. Dubovik, and B. N. Holben : Angstrom exponent and bimodal aerosol size  
22 distributions, J. Geophys. Res., 111, D07207, doi:10.1029/2005JD006328, 2006

23 Taha, G., Rault, D. F., Loughman, R. P., Bourassa, A. E., & Savigny, C. V. (2011).  
24 SCIAMACHY stratospheric aerosol extinction profile retrieval using the OMPS/LP algorithm.  
25 *Atmospheric Measurement Techniques*, 4(3), 547-556.

26 Thomason, L. W., Pitts, M. C., & Winker, D. M. (2007). CALIPSO observations of  
27 stratospheric aerosols: a preliminary assessment. *Atmospheric Chemistry and Physics*, 7(20),  
28 5283-5290.

29 Thomason, L. W., S. P. Burton, B.-P. Luo and T. Peter , SAGE II measurements of stratospheric  
30 aerosol properties at non-volcanic levels, *Atmos. Chem. Phys.*, 8, 983-995, 2008

1 Trepte, C. R., and Hitchman, M. H.: Tropical stratospheric circulation deduced from satellite  
2 aerosol data, *Nature*, Vol. 355, 626-628, 1992.

3 Trepte, C. R., Veiga, R. E., and McCormick, M. P. : The poleward dispersal of Mount Pinatubo  
4 volcanic aerosol, *J. Geophys. Res.*, vol. 98, No. D10, 18,563-18,573, 1993.

5 Trickl, T., Giehl, H., Jäger, H. and Vogelmann, H : 35 yr of stratospheric aerosol measurements  
6 at Garmisch-Partenkirchen: from Fuego to Eyjafjallajökull, and beyond. *Atmospheric*  
7 *Chemistry and Physics*, 13(10), 5205-5225, 2013

8 Vernier, J. P., Pommereau, J. P., Garnier, A., Pelon, J., Larsen, N., Nielsen, J., and McDermid,  
9 I. S., Tropical stratospheric aerosol layer from CALIPSO lidar observations. *Journal of*  
10 *Geophysical Research: Atmospheres*, 114(D4), 2009

11 Vernier, J.-P., Thomason, L. W., Pommereau, J.-P., Bourassa, A., Pelon, J., Garnier, A.,  
12 Hauchecorne, A., Blanot, L., Trepte, C., Degenstein, D., and Vargas, F.: Major influence of  
13 tropical volcanic eruptions on the stratospheric aerosol layer during the last decade, *Geophys.*  
14 *Res. Lett.*, 38, L12807, doi:10.1029/2011GL047563, 2011.

15 Winker, D., Vaughan, M., Omar, A., Hu, Y., Powell, K., Liu, Z., Hunt, Wand Young, S :  
16 Overview of the calipso mission and caliop data processing algorithms, *J. Atmos.1139 Oceanic*  
17 *Technol.*, 26, 2310–2323, 2009

18 Vignelles, D. : Caractérisation des performances du nouveau mini compteur de particule LOAC  
19 embarqué sous ballon météorologique : application à l'étude de la variabilité spatiale et  
20 temporelle des aérosols de la haute troposphère et de la stratosphère - PhD Thesis, Univ.  
21 Orléans, 2017

22 Weigel, R., Hermann, M., Curtius, J., Voigt, C., Walter, S., Böttger, T and Borrmann, S :  
23 Experimental characterization of the COndensation PArticle counting System for high altitude  
24 aircraft-borne application. *Atmospheric Measurement Techniques*, 2, 243-258, 2009

25 Wunderlich, F. and Mitchell, D. M : Revisiting the observed surface climate response to large  
26 volcanic eruptions. *Atmospheric Chemistry and Physics*, 17(1), 485-499, 2017

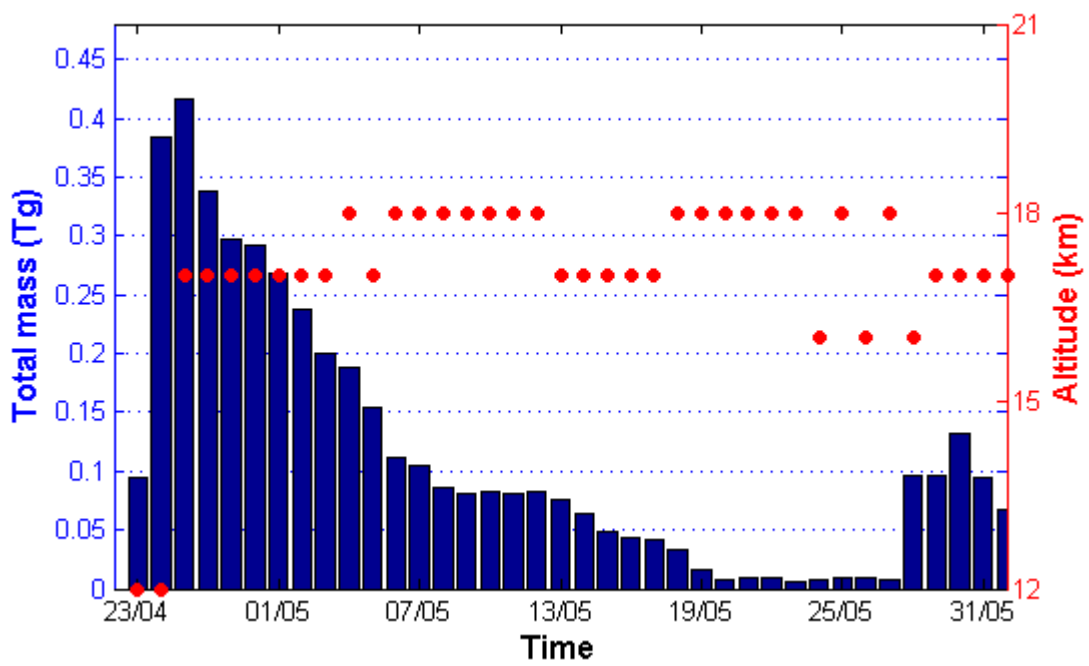
27 Xu, W., Jónsson, S., Ruch, J. and Aoki, Y : The 2015 Wolf volcano (Galápagos) eruption  
28 studied using Sentinel-1 and ALOS-2 data. *Geophysical Research Letters*, 43(18), 9573-9580,  
29 2016

1 Young, R., H. Houben, and O. Toon, Radiatively forced dispersion of the Mt. Pinatubo volcanic  
2 cloud and induced temperature perturbation in the stratosphere during the first few months  
3 following the eruption, *Geophys Res. Lett.*, 21, 369-372, 1994.

4 Zuev, V. V., Burlakov, V. D., Nevzorov, A. V., Pravdin, V. L., Savelieva, E. S. and Gerasimov,  
5 V. V.: 30-year lidar observations of the stratospheric aerosol layer state over Tomsk (Western  
6 Siberia, Russia). *Atmospheric Chemistry and Physics*, 17(4), 3067-3081, 2017

7

1  
2  
3  
4  
5  
6

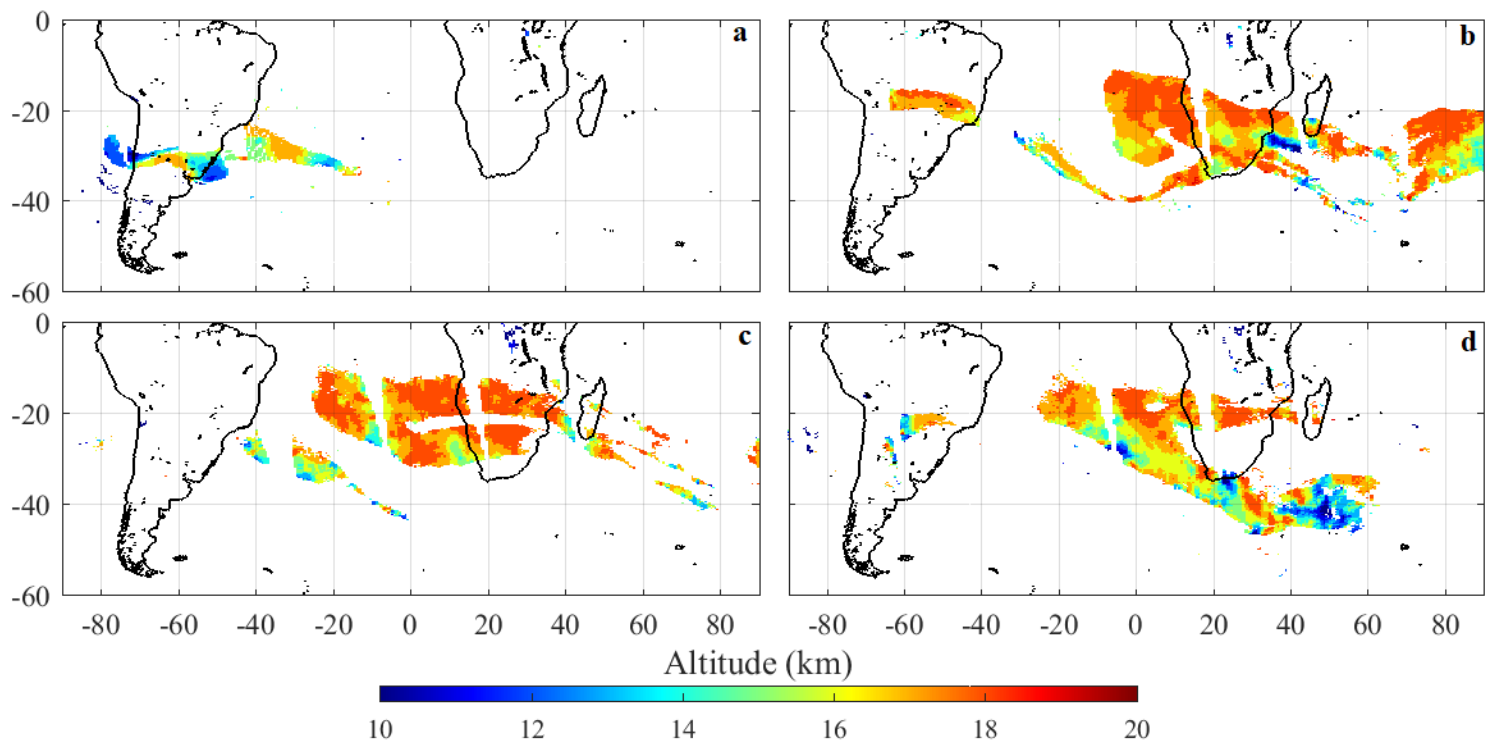


7  
8  
9  
10  
11  
12

**Figure 1 :** Evolution of the SO<sub>2</sub> total column mass (in blue) and the altitude of the maximum SO<sub>2</sub> mass (red dots) obtained from IASI from 23 April 2015 to 31 May 2015 over the southern hemisphere. The altitude of the maximum SO<sub>2</sub> mass was obtained from the algorithms detailed in Clarisse et al. (2014).



1  
2  
3  
4  
5  
6

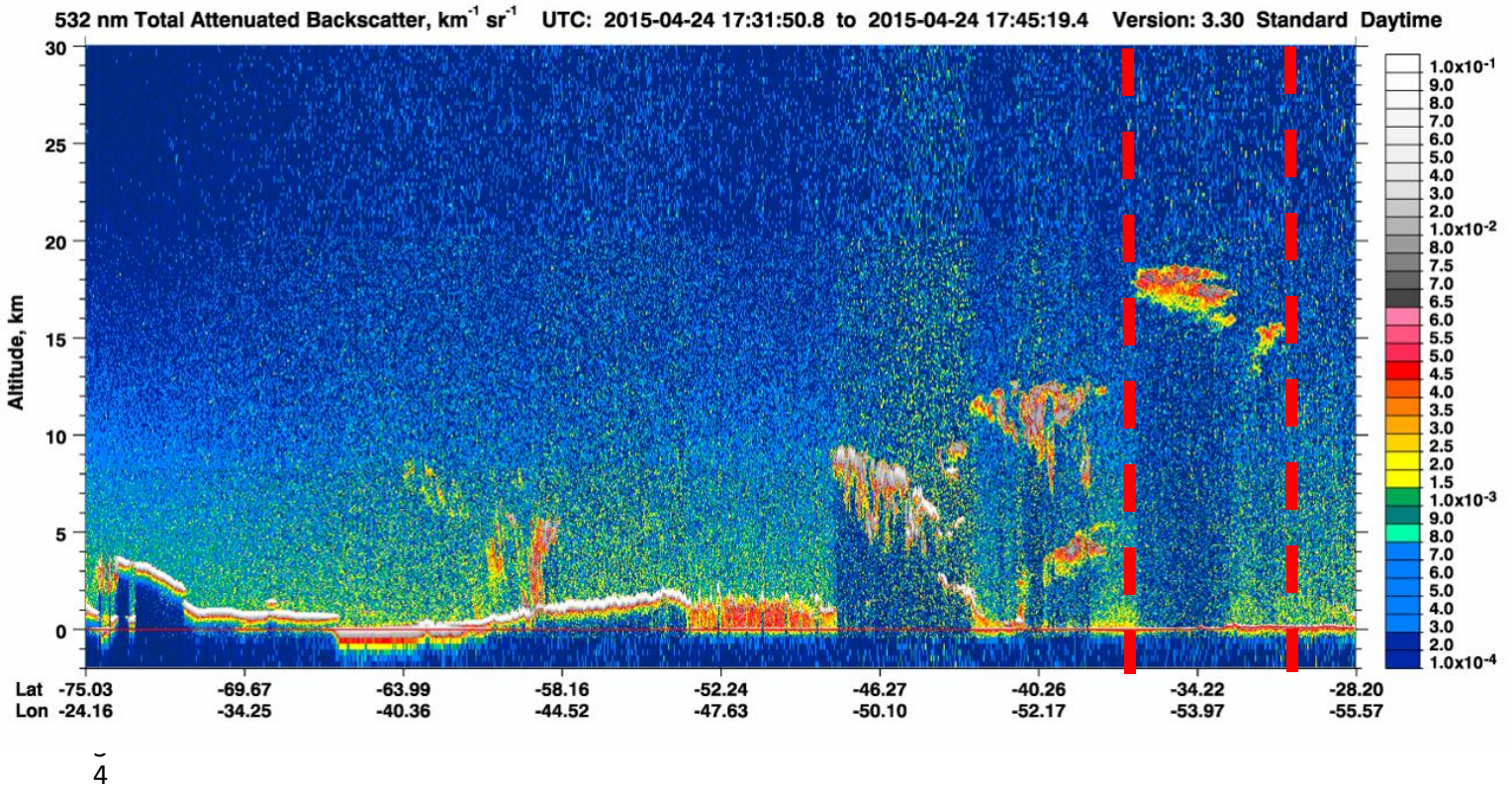


8 **Figure 2 : Injection Height (km)** and transport of SO<sub>2</sub> obtained from IASI observations during  
9 (a) 24/04, (b) 01/05, (c) 06/05 and (d) 11/05

10

1

2

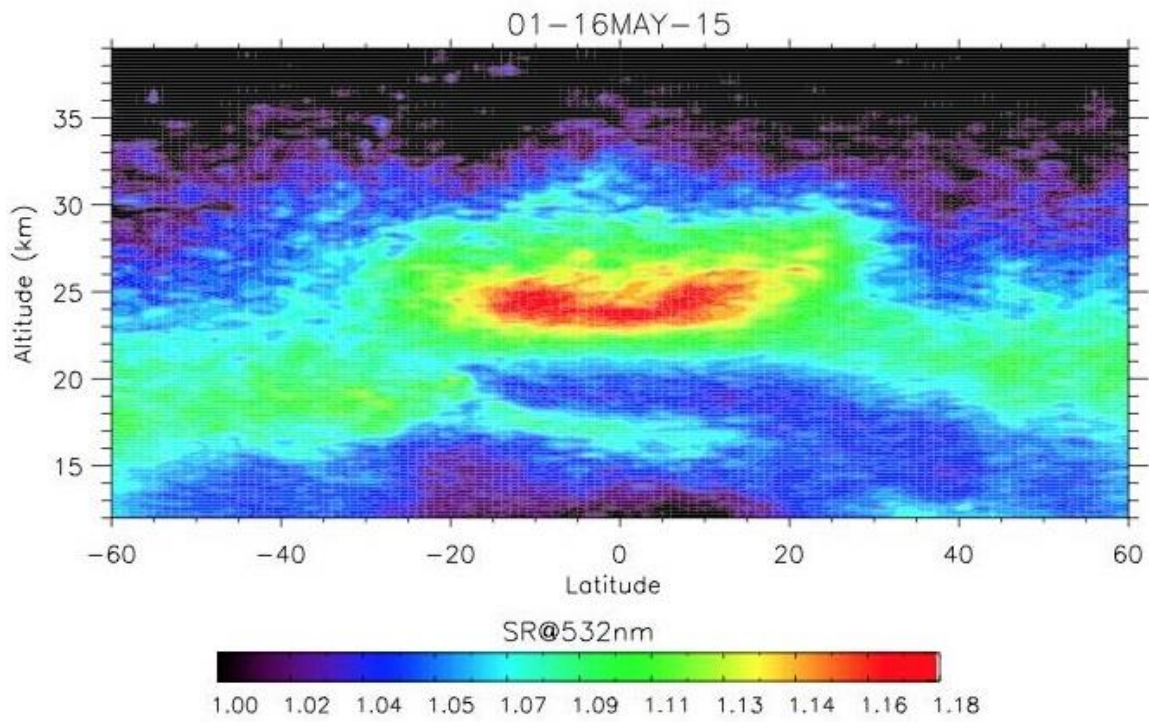


6 **Figure 3 :** CALIOP cross-section of 532 nm attenuated backscatter and Brightness temperature  
7 difference for the overpass at 1730-1745 on 24 April 2015 over the South America from 28°S  
8 to 75°S latitude range. The two red dash lines delimited the geographical region where the  
9 Calbuco plume is observed by CALIOP on 24 April 2015.

10

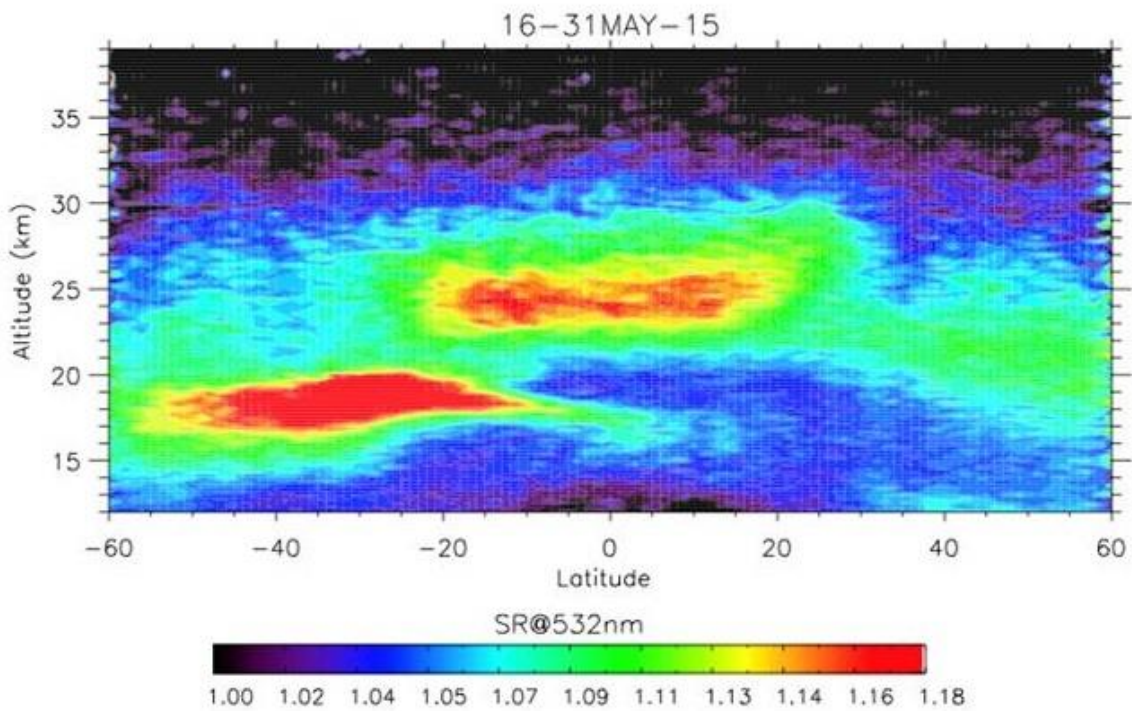
1

2 a)



3

4 b)



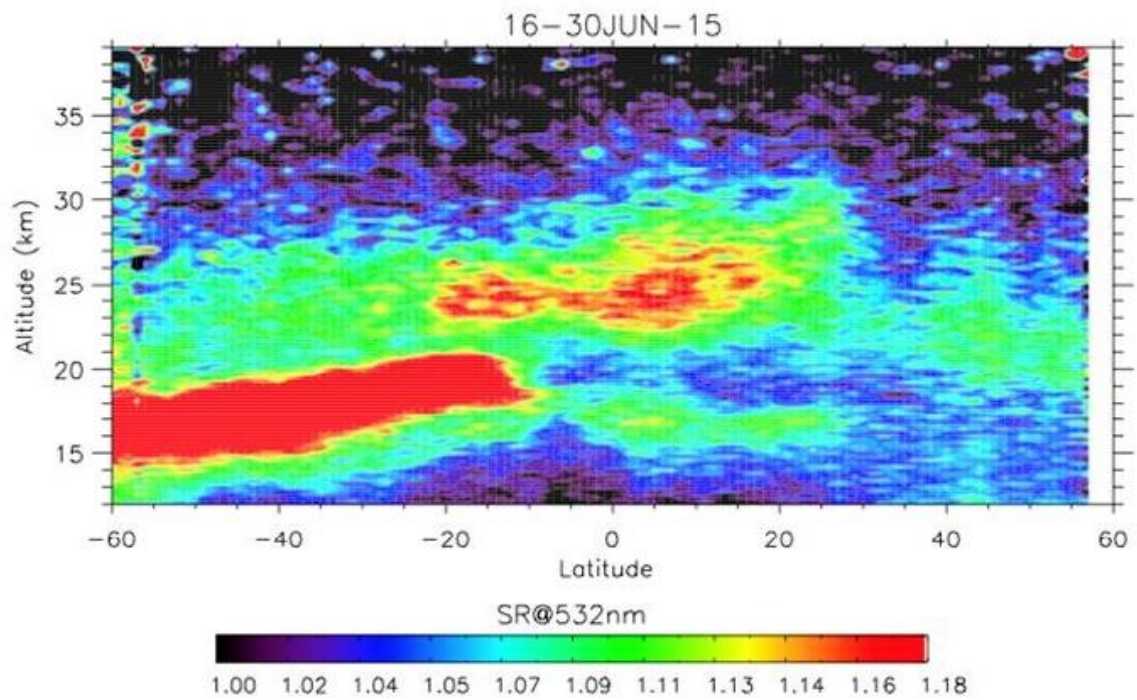
5

6 **Figure 4** : Half monthly mean of the zonal scattering ratio at 532 nm in (a) 1-15 May (1-2  
7 weeks after eruption), (b) 16-31 May (3-4 weeks after eruption).

8

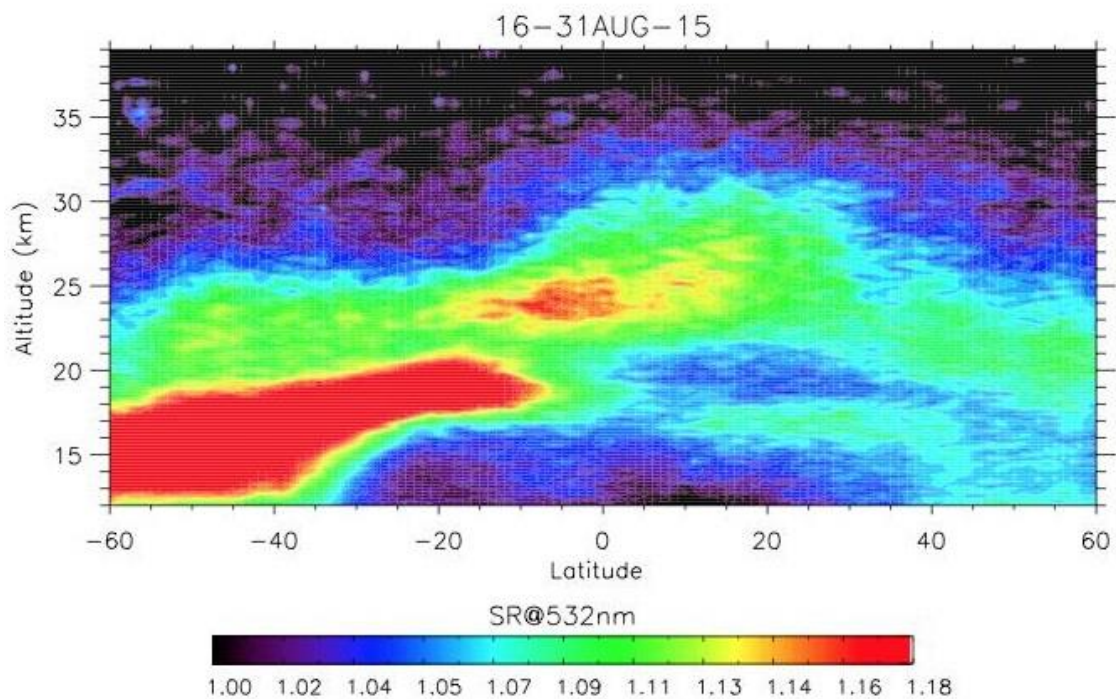
1

2 a)



3

4 b)

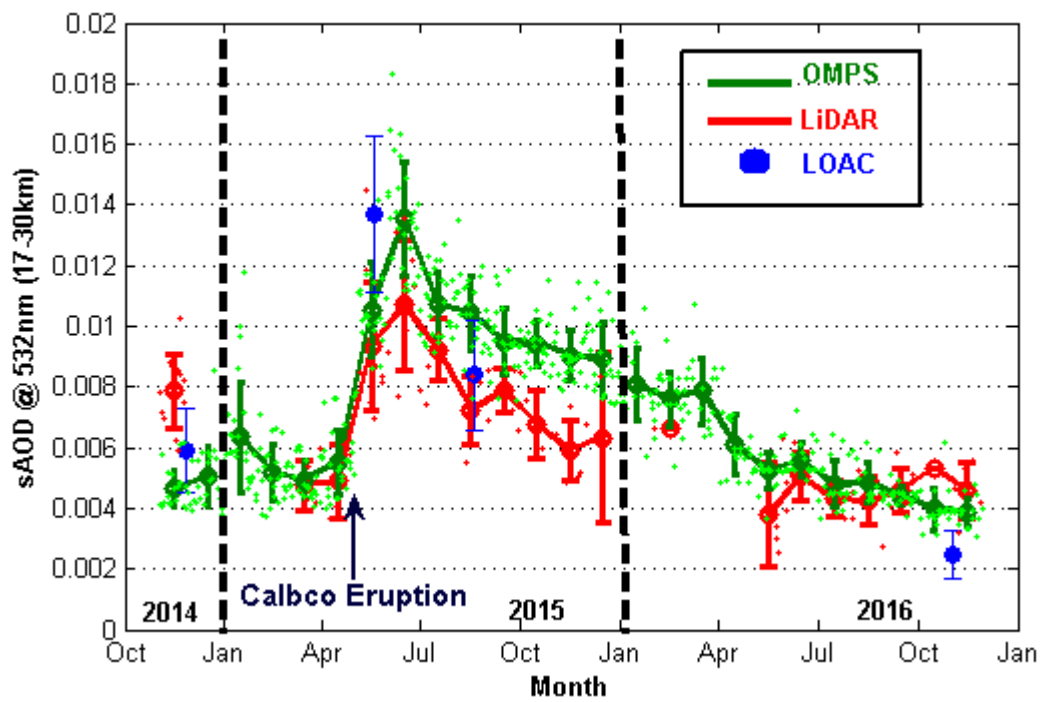


5

6 **Figure 5** : Half monthly mean of the zonal scattering ratio at 532 nm in (a) 16-30 June (2  
7 months after eruption) and (b) 16-31 August (4 months after eruption).

8

1  
2  
3  
4  
5

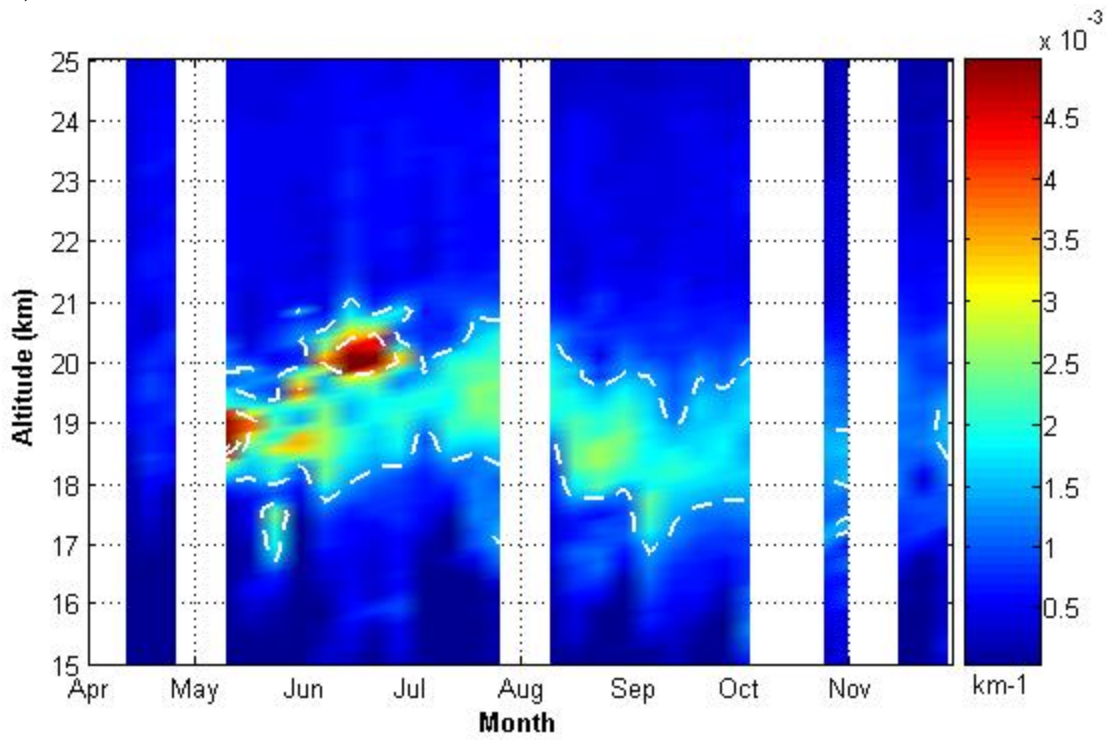


6  
7  
8  
9  
10  
11  
12  
13  
14  
15  
16

**Figure 6 :** Evolution of sAOD calculated between 17 and 30 km at 532 nm from LiDAR (red), LOAC OPC (blue) and OMPS (green) observations between November 2014 to November 2016 over the Reunion site. The small dots represent the daily sAOD and the large dots represent the monthly averaged sAOD obtained from OMPS and LiDAR observation. The large blue dots represent the sAOD calculated from LOAC OPC observations over Reunion during the 26 November 2014, the 19 May 2015, the 19 August 2015 and the 2 November 2016. The error bars associated to LiDAR and OMPS observations represent the standard deviation. The error bars associated to LOAC OPC represent the uncertainties values. The date of the Calbuco eruption is indicated by a blue arrow.

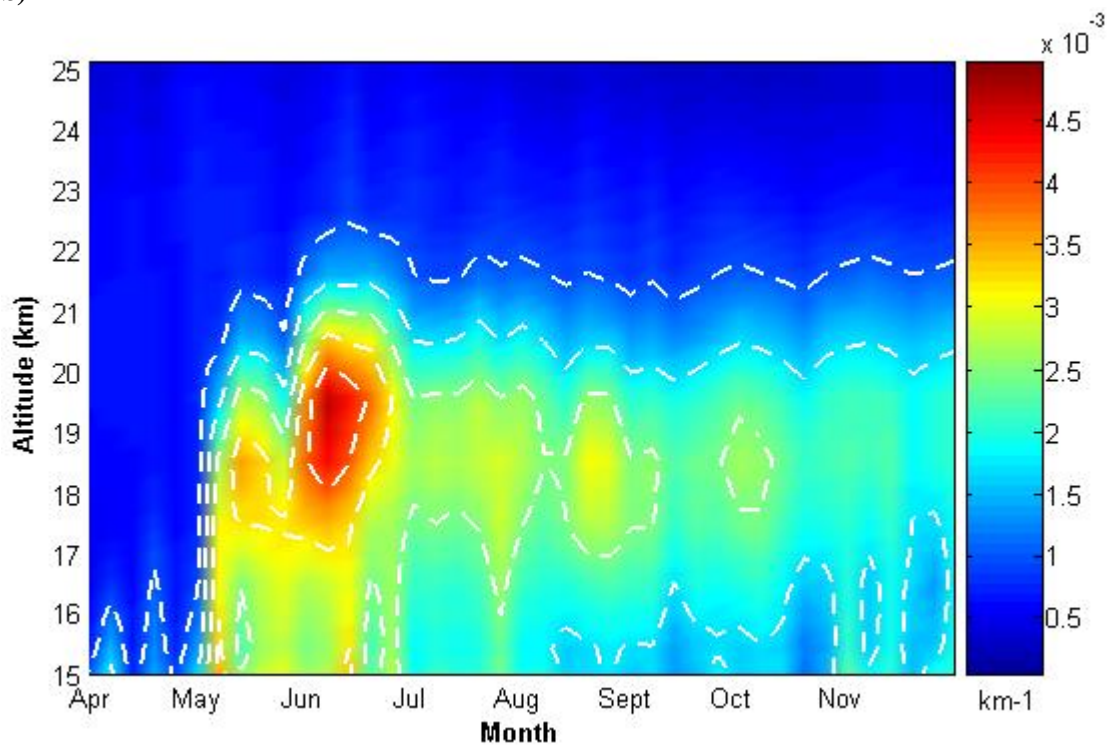
1

2 a)



3

4 b)

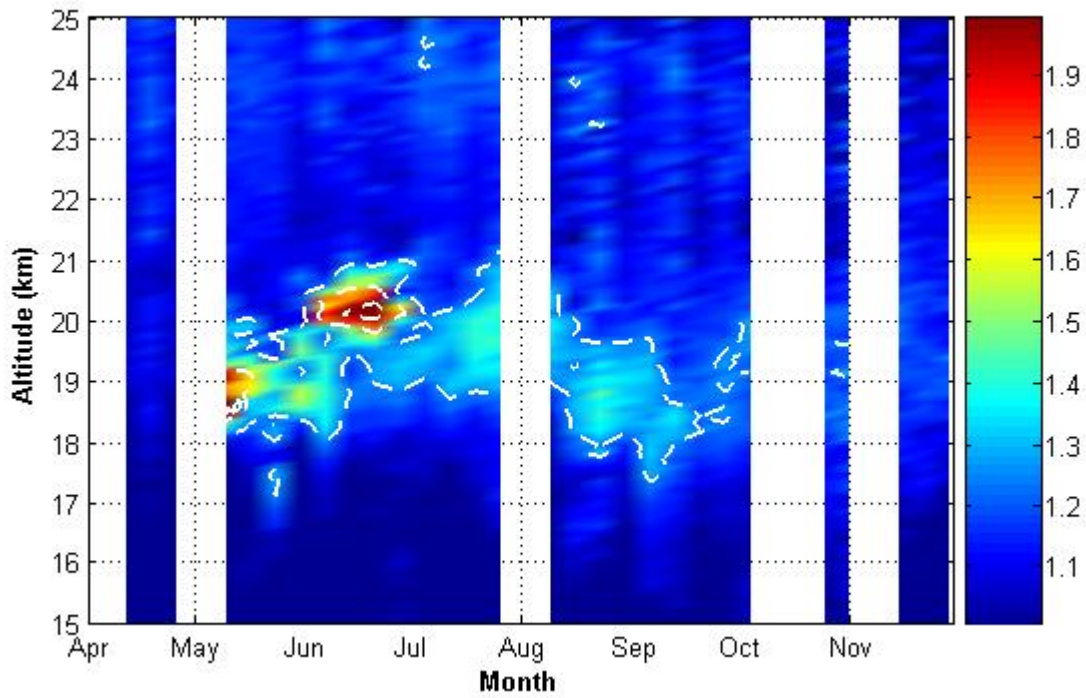


5

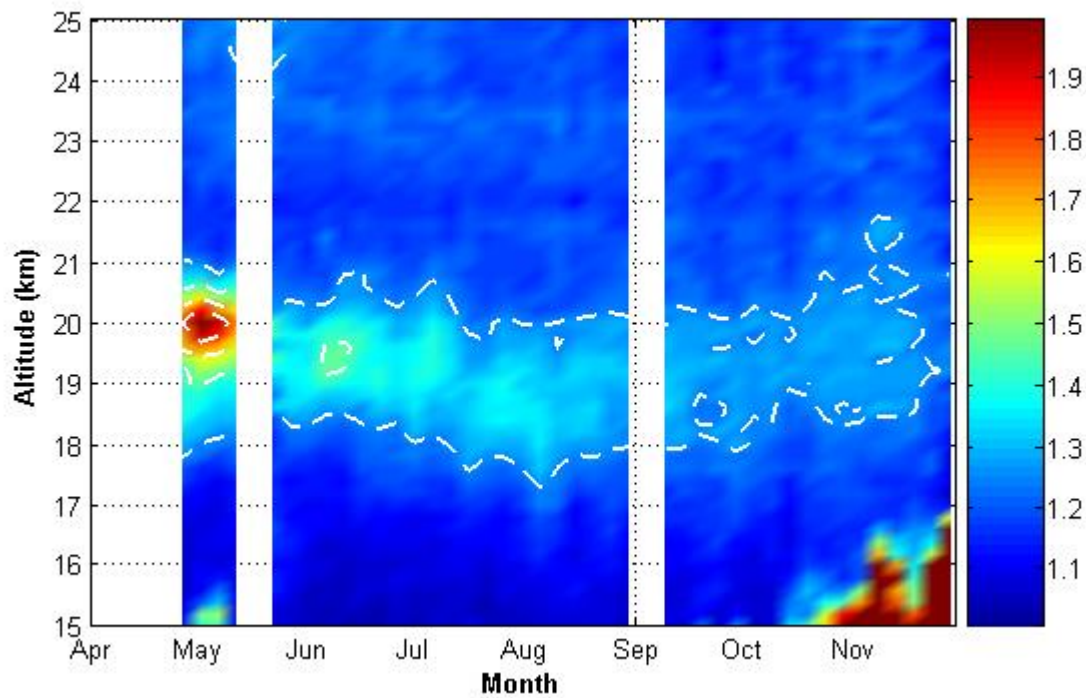
6 **Figure 7 :** Time series of weekly-averaged profiles of extinction at 532 nm obtained from (a)  
7 lidar and (b) OMPS observations over Reunion between April 2015 and December 2015.

8

1 a)



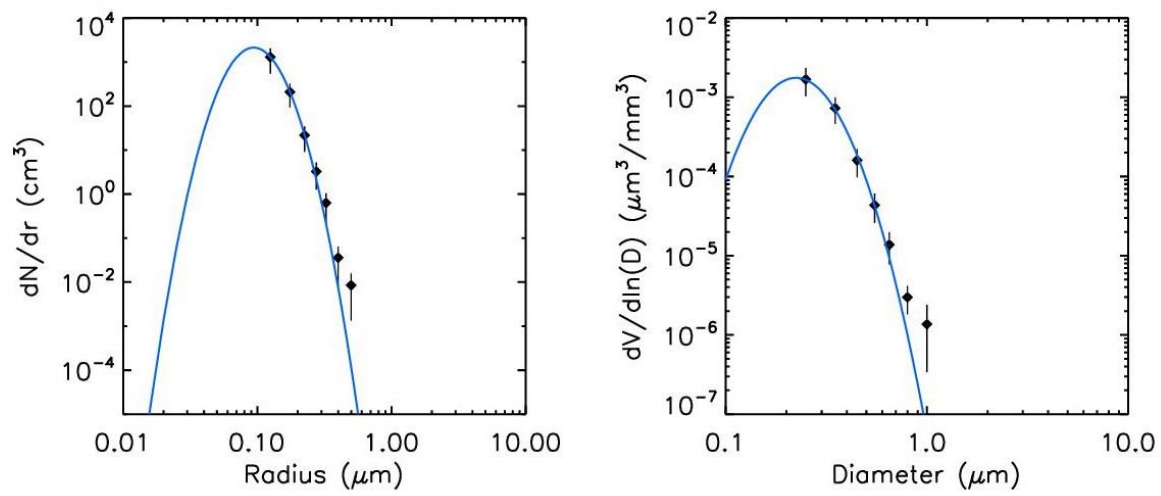
2  
3 b)



4

5 **Figure 8 :** Time series of weekly-averaged profiles of scattering ratio at 532 nm obtained from  
6 **ground-based (a) and space-borne (CALIOP, b) LiDAR observations over Reunion Island**  
7 between April 2015 and December 2015. The scattering ratios from CALIOP have been  
8 averaged within  $\pm 5^\circ$  in latitude and  $\pm 50^\circ$  in longitude (extending from Africa to Australia)  
9 around Reunion Island.

1  
2  
3  
4  
5  
6

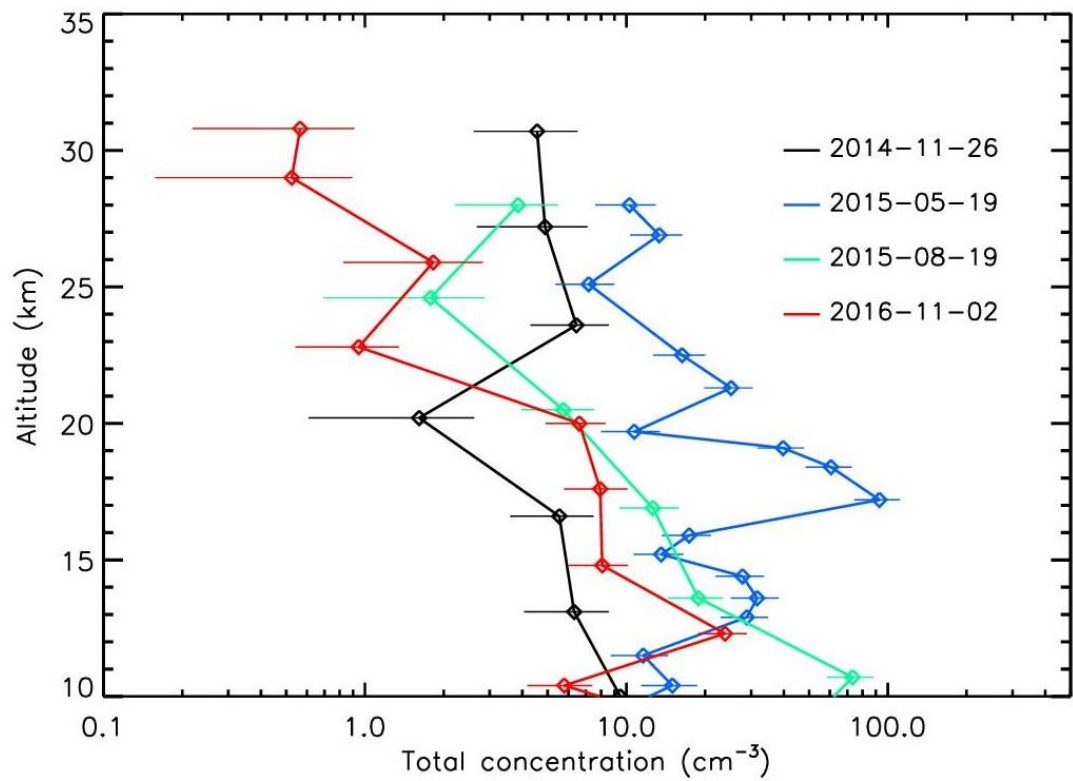


7  
8  
9  
10

**Figure 9** : Number ( $dN/d\ln(D)$ ) and Volume concentration ( $dV/d\ln(D)$ ) obtained from LOAC OPC observations on 19 May 2015 at 1746 UTC over the Reunion site.



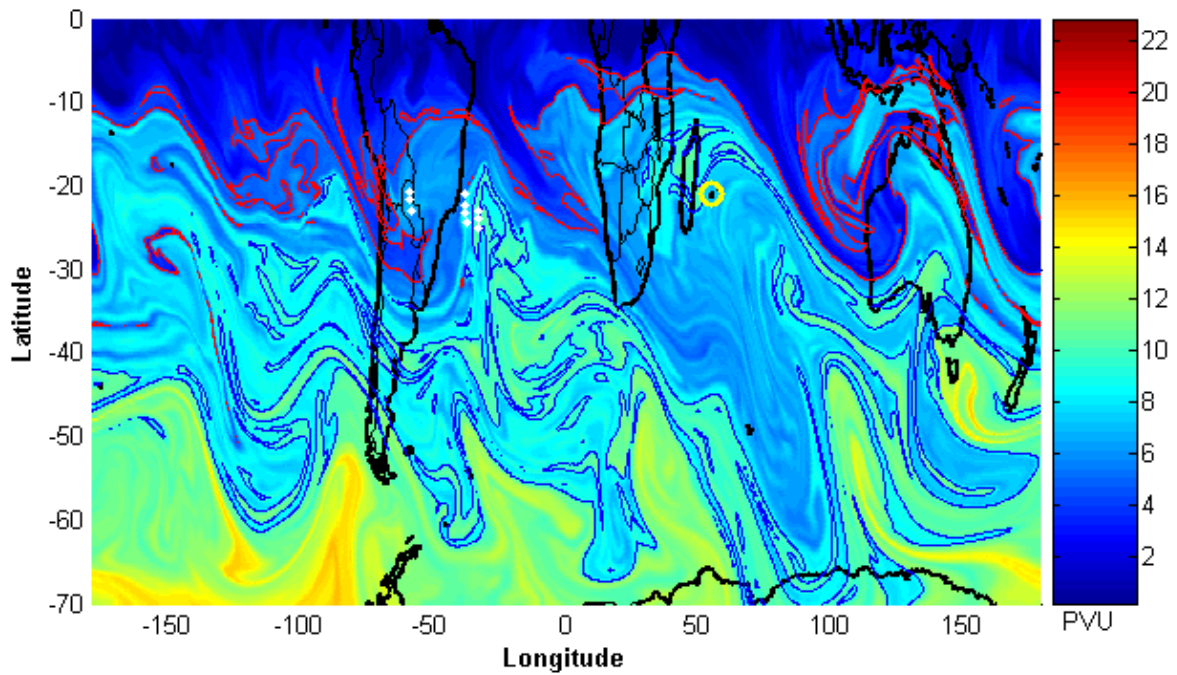
1  
2  
3  
4  
5  
6



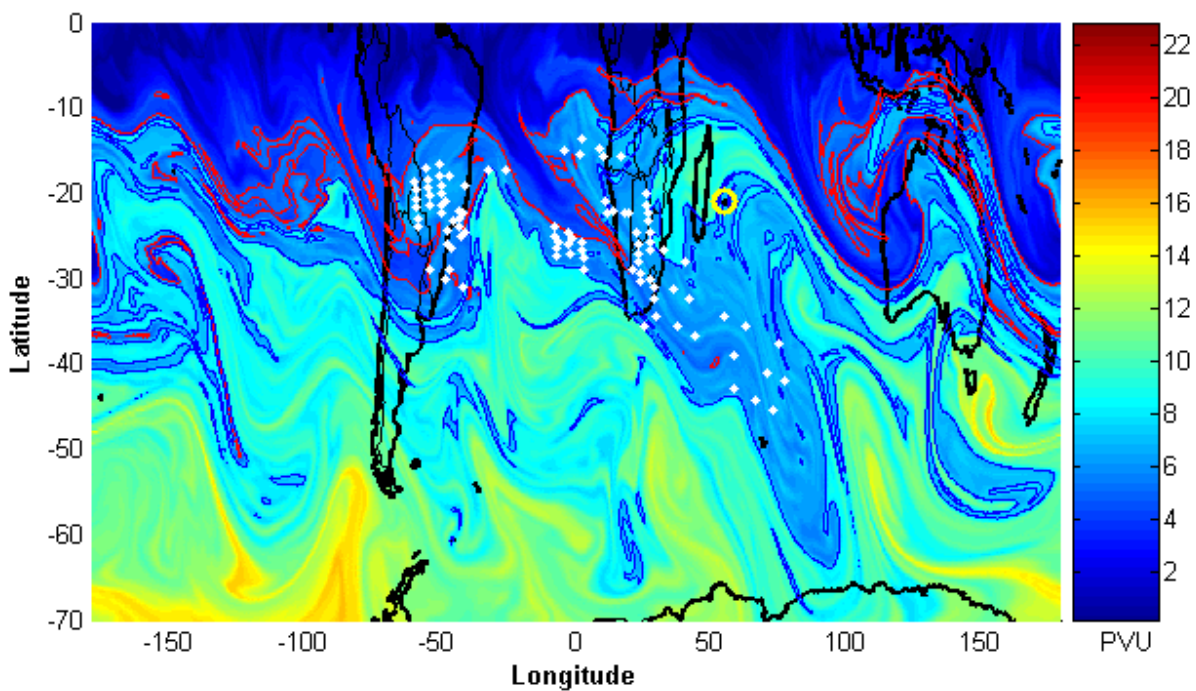
7  
8  
9  
10  
11  
12

**Figure 10 :** Total number concentration of aerosols (0.2-50 $\mu$ m) profiles obtained from LOAC OPC observations over Reunion during the 26 November 2014 (black line), the 19 May 2015 (blue line), the 19 August 2015 (green line) and the 2 November 2016 (red line). The aerosols layer is delimited by two horizontal black lines.

1 a)



2  
3 b)

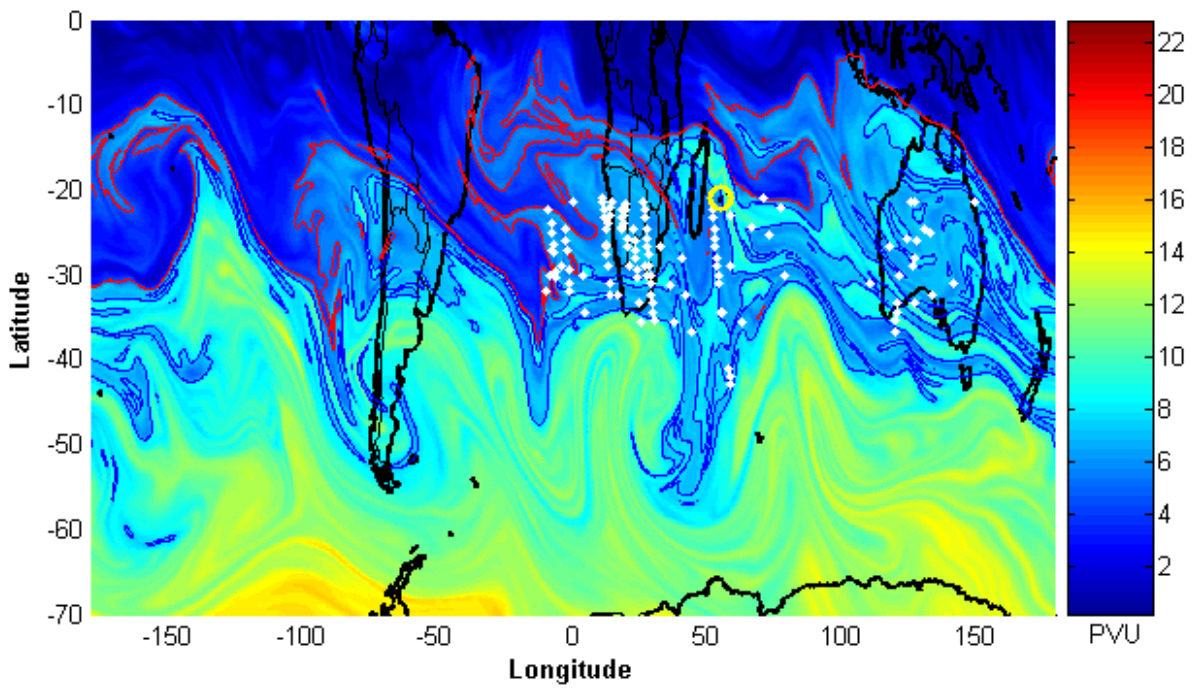


4

5 **Figure 11** : Advected PV map at the 400 K level obtained from the MIMOSA model (a) on 27  
6 April 2015 and (b) on 01 May 2015. The positions of the subtropical barrier (red line) and a  
7 south dynamical barrier (blue line) are detected from the DyBAL code. The white dots represent  
8 the localization of the aerosol plume at  $400 \text{ K} \pm 5 \text{ K}$  obtained from OMPS observations, while  
9 the yellow circles indicate the Reunion site.

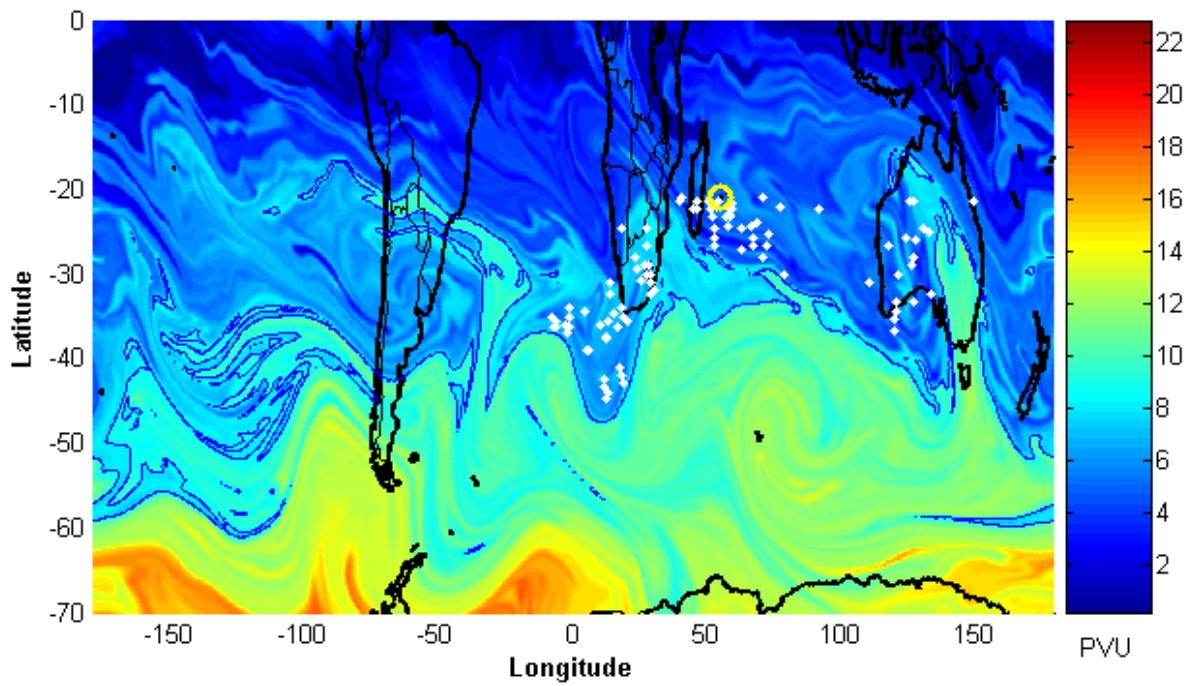
10

1 a)



2

3 b)



4

5 **Figure 12:** Same as Figure 11 but for (a) 19 May 2015 and (b) 03 June 2015.

6

7